Modification of solids with ultrashort pulses Time resolved spectroscopy

Gautier Vilmart

August 2014

Degree project in enginerring physics
CEA, Saclay

Modification of solids with ultrashort pulses : time resolved spectroscopy

Gautier Vilmart

Examiner : Professor Valdas Pasiskevicius
Supervised by Stéphane Guizard

Master Thesis report
Degree program in Engineering Physics

KTH
Sweden

Laboratoire des Solides irradiés
CEA Saclay
France

2014
TRITA-FYS 2014:61
ISSN 0280-316X
ISRN KTH/FYS/–14:61-SE

Introduction

The recent evolution of the femtosecond laser technology has made possible the use of very short and energetic pulses, which has opended a wide range of new experiments that has led to new understandings of the matter and of the light-matter interaction. In dielectrics, the discovering that pulses under 250 fs and under 1.6 µJ can modify permanently the refractive index without breaking the material has lead to new applications such as Bragg gratings in SiO_2[1][2][3]. At higher energies, very precise 3D nano processing inside the bulk has been shown possible[2][4][5][6]. Despite those practical achievement, the physical mechanisms are still not fully undestood. Indeed, the light-matter interaction mecanisms are different than the ones at longer time pulses[7]. When at picosecond laser pulses the main effects are thermal, it is not the case for femtosecond pulses. In this master thesis, we will focus on the interaction between femtosecond laser pulses and dielectrics such as fused silica and sapphire. First, the underlying theories will be briefly recalled. Then, we will present the differents experimental setups that make us possible to follow the excitation and relaxation of electrons on very short time scales, and on longer time scale. In addition to the experimental results, we will also present the new results we obtained thanks to numerical simulations, and show how those results draw a different pictures of the light-matter interraction with ultrashort pulses that the one commonly accepted.

Contents

List of Figures

Chapter 1

Theory

1.1 Backgound

1.1.1 The free electron Drude model

This model has been developed by Paul Drude in 1900. It has been developed in analogy with the gas kinetic theory and applied to the electrons in metals. Indeed, the electrons are considered in this model as a gas of particles accelerated by the magnetic and electric fields, and slowed by collisions with the atoms cores. Though it has been proved that it was based on false hypotheses, the model still gives surprisingly good predictions, and gives an explanation to some characteristics of metals such as electric conductivity, thermic conductivity and Hall effect.

The hypotheses

The hypotheses in the Drude model are :

- The negative charge carriers are electrons that behave as a gas on which the kinetic theory can be applied.
- The positive charge carriers can be considered as not moving because they are a lot heavier.
- There are no interactions between electrons. The electrons can be described classically.
- Collisions are instantaneous, and modify the speed of electrons instantaneously. The probability there is a collision between t and t+dt is given by $\frac{dt}{\tau}$ where τ is the mean time between two collisions.

Determination of the refractive index with the Drude-Lorentz model [8]

The goal of the Drude-Lorentz model is to model the interaction between light

and an atom with a single resonant frequency. The displacement of the atom is calculated as :

$$m\frac{d^2x}{dt^2} + m\omega_c\frac{dx}{dt} + m\omega_0^2 x = -eE$$

where m is the mass of the electron, ω_c a damping term representing the loss of energy by collisions of the atom, and ω_0 is the atom resonant frequency. Let's now describe the light :

$$E(t) = E_0 cos(\omega t + \Phi) = E_0 \Re(e^{-i(\omega t+\phi)})$$

where ω is the frequency of the light. When incorporating the latter equation on the first, we find that :

$$x(t) = -\frac{eE_0/m}{\omega_0 - \omega^2 - i\omega\omega_c}e^{-i\omega t}$$

The resonant polarization created by the dipoles due to the displacements of the atoms from their equilibrium can be caluclated as :

$$P_{resonant} = \frac{Ne^2}{m}\frac{1}{(\omega_0^2 - \omega^2 - i\omega\omega_c)}E$$

where N is the number of atoms per unit volume. This can be used to calculate the relative dielectric constat ε_r. From the Maxwell's equation, we know that :

$$\begin{aligned} D &= \varepsilon_0 E + P \\ &= \varepsilon_0 E + P_{background} + P_{resonant} \\ &= \varepsilon_0 E + \varepsilon_0 \chi E + P_{resonant} \\ &= \varepsilon_0 \varepsilon_r E \end{aligned}$$

where we assumed in the last relation that the material is isotropic. χ is the electric susceptibility. This gives us :

$$\varepsilon_r(\omega) = n^2(\omega) = 1 + \chi + \frac{Ne^2}{\varepsilon_0 m}\frac{1}{(\omega_0 - \omega^2 - i\omega_c\omega)}$$

In the free electron model, the electrons are not bound to the nucleus, which means that in this case, $\omega_0 = 0$. For $n_0 = 1 + \chi$, we have :

$$n^2(\omega) = \varepsilon_r(\omega) = n_0 - \frac{Ne^2}{\varepsilon_0 m}\frac{1}{(\omega^2 + i\omega_c\omega)}$$

This relation will prove usefull in the next of the report.

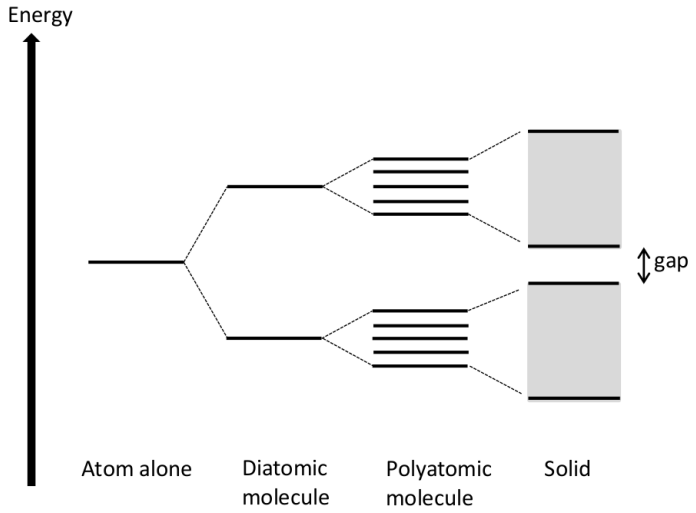

Figure 1.1: Origin of the bands

1.1.2 The band theory

The band theory derives from the orbital theory. It describes the different energies an electron can take inside a solid. Contrarily to the cases of a single atom or of a polyatomic molecule, the energy is not discretised, meaning that the energy of an electron can lie on a large continuous range of energy called band. Some values of energy are still not accessible ; those form a band called forbidden band. The origin of those continuous bands comes from the interactions between the orbitals of the atoms inside a large, periodic lattice of atoms or molecules. This is depicted in Fig.1.1. The theory has been successful in explaining some phenomena such as electrical resistivity and optical absorption.

One other achievement of this model is explaining the difference between metals, semiconductors and insulators :

- Metals : the electrons partially occupy the conduction band, and can thus circulate freely on the material under optical or thermal excitation.
- Semiconductor : The valence band, where all the electrons are initially, and the conductor band are separated by a forbidden band, also known as a gap, which prevents the electrons to circulate freely. Only excitations with energy higher than the band gap can promote the electrons in the conductor band. This can be achieved under visible light excitation for E_g of the order of 1 or 2 eV.
- Insulator, or dielectric : In this case, the bandgap is a lot larger (around 10 eV). This means that it is not possible under usual thermal excitation or

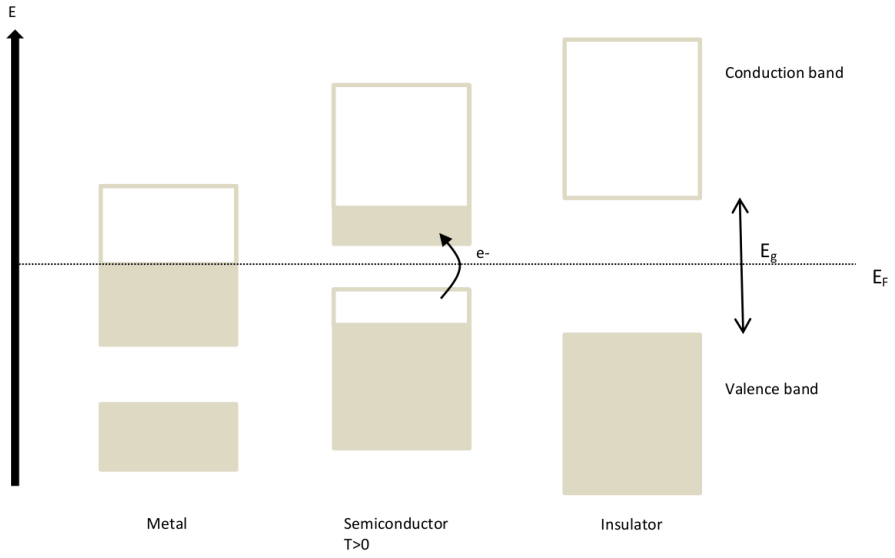

Figure 1.2: Difference between metal, semiconductor, and insulator

linear visible light excitation to promote electrons in the conductor band.

The difference between the three types of matter is shown in Fig.1.2.

In this thesis we will discuss only about dielectrics. We will see that although it is not possible for one single photon in the visible range to cross the bandgap, some non-linear mechanisms make possible the excitation of electrons under high intensities.

1.1.3 The phonons

Any vibration of the lattice of a crystal can be decomposed into a linear combination of normal modes of oscillations of the atoms, based on the symetry of the system. All those modes can propagate along a wave vector k at a frequency ν, and it is possible to associate to them an energy $E = h\nu$ and a momentum $p = \hbar k$. As we see, it is analog to the photon case, which is why the wave packet is said to be a quasiparticle, the phonon. They are responsible for a lot of different phenomena in solids such as heat capacity, thermic conductivity or electric conductivity.

Two types of phonon exist, acoustic phonons and optical phonons, the difference between the two being that although acoustic phonons implies the relative motion of atoms inside the primitive cells around, optical phonons only implies the relative motion of atoms inside one primitive cell, which means that only a crystalline system with more than one atom per cell can have optical phonons. This is illustrated in Fig.1.3. The names of those phonons come from

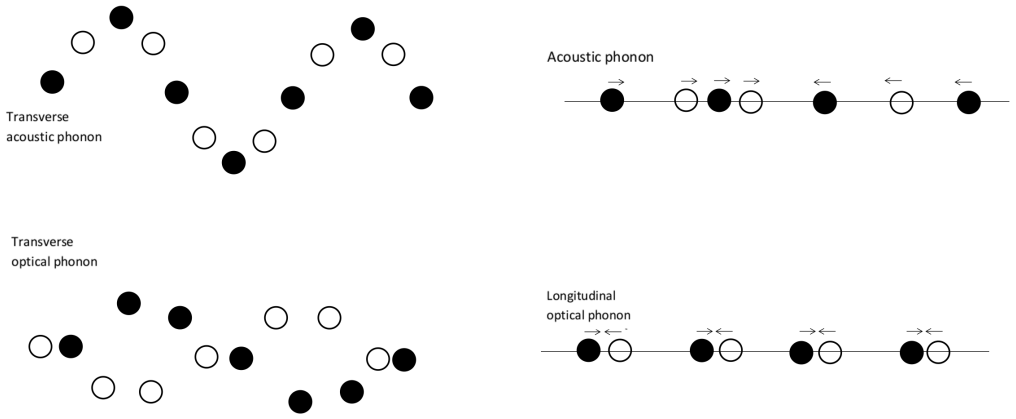

Figure 1.3: The different types of phonons. One primitive cell is composed of one white and one black atoms.

the fact that acoustic phonons correspond typically to the sound waves propagating inside the material, and the optical phonons are easily excited by infrared radiation. Those are the type of phonon we are most interested in this master thesis.

1.1.4 The Self Trapped Electron (STE)

In SiO_2, under high intensities of light, some defects are created [9]. Those intrinsic defects called Self Trapped Excitons (STE) are the results of the trapping of an electron on a silicon atom, and a hole on an oxygen atom[10]. That makes the oxygen atom move to an interstitial position (movement of $0.4\mathring{A}$). Those movement are shown in Fig.1.4. This creates two levels of energy in the band gap, at 2,6 eV and 5,2 eV [10]. Althouth the STE are among the best studied radiation induced defects, some of its property are not known yet. For example, its lifetime had never been studied before this experiment.

1.2 Light-matter interactions in wide-bandgap dielectrics

The wide-bandgap of the materials we studied (around 10ev) makes it impossible to have direct transition from the valence band to the conduction band under normal conditions unless using an exemer laser. However, under high intensities those transitions are made possible, thanks mostly to two mechanisms : multiphoton ionization and electronic avalanche. The latter, although very efficient once triggered, needs a preexcitation of the material, so it is generally assumed that the former is responsible for the initial excitation of electrons[7].

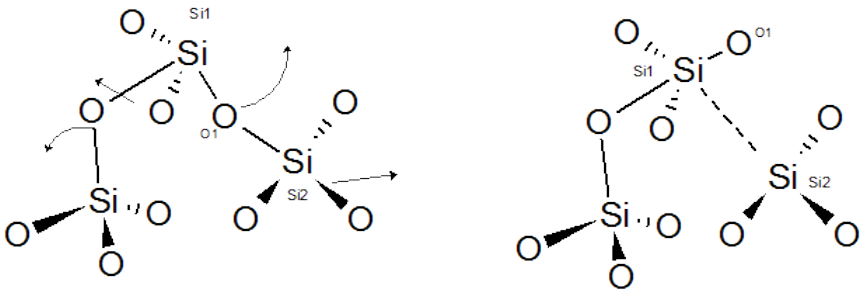

Figure 1.4: STE. One electron is trapped on Si1, and one hole on O1. This makes the O1 oxygen atom move to an interstitial position. As a result, the O1-Si2 bound is very weak.

However, their respective contribution is still under debate. In particular, previous studies in our research group tend to show that in some materials such as Al_2O_3, their might not even be any electric avalanche [11][12]. This will be discussed later. Other mechanisms can have a huge importance, such as defect-assisted ionization, where the presence of defect states lower the multiphoton absorption order[13]. For this reason, the material used is very pure.

1.2.1 Electrons excitation mechanisms

Multiphoton ionization

It is possible at high intensities to have simultaneous absorption of n photons, which can results in the excitation of some electrons if the total energy is greater than the bandgap. It is a non-linear process, being a n^{th} order dependency of the laser intensity. The multiphoton transition probability per time unit W can be written as [14]:

$$W = \sigma_n F_p^n$$

with σ_n being the generalized cross section for N-photon transitions (in $cm^{2N}s^{1-N}$) which can empiricaly be estimated by $\sigma_n \approx 10^{-19}.(10^{31\pm2})^{1-N}$, and F_p being the photon flux density of the pump defined as $F_p = \frac{I_p}{\hbar\omega}$ where I is the intensity of the pulse and ω is its angular frequency. Let's now express the probability of multiphoton absorption per irradiated surface unit P :

$$P_v = N_v\sigma_n(\frac{F}{\hbar\omega\tau})^n\tau$$

where N_v is the number of electrons in the conduction band, and τ is the pulse duration, and F is the laser intensity (in $J.cm^{-2}$). We see that for n>2, short pulses favor this mechanism.

Electron heating and impact ionization

Once in the conduction band, the electrons which are at first in the bottom of

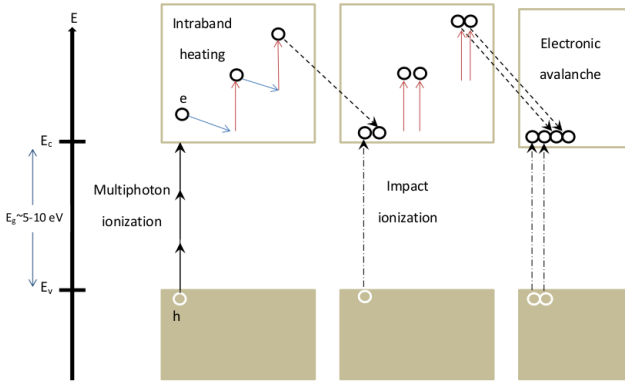

Figure 1.5: Schema of multiphoton ionization and impact ionization

the band can be further excited by a mechanism called "inverse Bremsstrahlung". It consists in a three-body interaction between the electron, a photon and a phonon, and it results in the raise of the kinetic energy of the electron.

Once a critical density of electron is in the conduction band and the energies of the electrons are high enough, a new mechanism called impact ionization can occur. It consists in the collision of a high energy electron and an electron in the valence band, thus promoting the latter in the conduction band. It is a very efficient way of promoting electrons, the density of electrons increasing in an exponential rate. In bands with parabolic dispersion, this mechanism starts to be in action for energies such as [15]:

$$E_{imp} = (\frac{1+2\mu}{1+\mu})\tilde{E}_g$$

with $\mu = \frac{m_c}{m_v}$is the ratio between the effective masses of the conduction and valence band. For SiO_2, this value is often greater than 13.5 eV, which means that an electrons irradiated by 800nm photons have to undergo 9 inverse Bremsstrahlung before impact ionization can occur. This is a very high value and the importance of this process is still under debate.

The two mechanisms are depicted in Fig.1.5.

1.2.2 Electrons relaxation mechanisms

The electrons in the conduction band are cooled by radiative and non-radiative processes, namely scattering, which can occur between one electron and a phonon, an ion, or another electron. In SiO_2, it has been showed that acoustic phonons are responsible for the momentum relaxation, while optical phonons are prominent for electrons energies from 0 to 5 eV [16]. Above this value, electron-electron scattering is the most efficient mechanism. The radiative cooling takes place at much longer delay (around 1 ns). Alternatively, electrons can be trapped. Extrinsic trapping occurs when there are imperfections in the material. Intrinsic trapping, that is to say trapping induced by light-matter interaction also plays a role in some materials such as quartz[17]. One of the most studied intrinsic trap is STE (Self Trapped Electron), which corresponds to a distortion of the lattice. We will see that this induced defect plays an important role in our experiment.

1.2.3 Phonons excitation mechanism

Optical phonons in a transparent medium can be excited by light through a mecanism called stimulated Raman scattering. As a reminder, Raman scattering in general describes the process by which when scattered by an atom, some photons are not elastically scattered at the same energy as the excitation photons as most are, but scattered with a different energy, often lower (Stokes Raman scattering), and sometimes higher (anti-Stokes Raman scattering). This results from an exchange of energy between the radiation and the medium.

What we described happens spontaneously (spontaneous Raman scattering), but when Stokes photons are injected in a media together with the original light, it is possible to have a rate of scattering higher than that of spontaneous Raman scattering, resulting in an amplification of the Stokes signal. The original light works as a pump in a laser. This effect can be used to create Raman amplifier and Raman lasers.

The condition for stimulated Raman scattering is using two laser pules of frequencies ω_1 and ω_2 choosen so that $\omega_2 - \omega_1 = \omega_0$ where ω_0 is the frequency of the Raman mode [18].

Let's now describe the mecanism mathematically : starting from the classical harmonic oscillator, the movement equation of the phonon is :

$$\frac{\partial^2 Q}{\partial t^2} + 2\gamma \frac{\partial Q}{\partial t} + \omega_0^2 Q = F(t)$$

where Q is the deviation of the internuclear distance from its equilibirum Q_0, γ is a damping term, and ω_0 is the frequency of the Raman mode. The key assumption of the theory is that the optical polarizability of the molecule is not constant but depends on the internuclear separation $Q(t)$ acording to the following equation [19]:

$$\alpha(t) = \alpha_0 + \left(\frac{\partial \alpha}{\partial Q}\right)_0 Q(t)$$

For a Gaussian pulse described as :

$$E = Ae^{-(t-zn/c)^2/(2\tau_l^2)}cos(\omega_l(t - zn/c))$$

where A is the amplitude of the electrical field, τ_l is the length of the pulse and ω_l is the central frequency of the pulse, is can be shown that the amplitude of the phonon Q_0 is equal to :

$$Q_0 = \frac{2\pi I\, N\bar{\alpha}}{\omega_0 nc} e^{-\omega_0^2\tau_l^2/4}$$

where I is the fluence of the excitation pulse, N is the number of oscillators per volume unit and $\bar{\alpha} = (\partial\alpha/\partial Q)_0$.

As we see, the excited phonon is described by a damped sinusoide. Furthermore, another point we might stress is that the phonons oscillations are generated by a pulse much quicker than their vibration frequency. This means that the oscillations are generated coherently, that is to say that the vibration wave of the phonon is known.

1.3 Modification regimes

The different regions The interractions bewteen light and the material lead to different outcome for severals light conditions. Depending on the energy of the pulse and of its duration, several regimes have been observed[1]. The pulse energies and durations at which they can be found is plotted in Fig.1.6. In region 1, the pulse energy is too low to induce any modification and damages. In region 3, the pulse is powerfull enough to induce damages. In region 2, that is to say for pulse duration under 260 fs and for its enegy between 0.3 and 1.6 µJ, the refractive index is changed, without ablation of the material. Two different regimes have been observed in this region : smooth refactive index change, and birefringent refractive index change. Several theories has been suggested in order to explain smooth refractive index change[2]. In the thermal model, a small volume of the material is heated to very high temperature. The subsequent quenching of the material change its density, thus changing the refractive index. However, it has been shown that it is not the only mechanism. Other phenomena such as the appearance of color centers , and the densification of the material due to structural changes can explain smooth refractive index change.

Because of those different regimes, the boundary between region 1 and region 3, and the boundary between region 2 and region 3 is called the damage threshold. The boundary between region 1 and region 2 is called the modification threshold.

Ablation criteria In order to model the interaction, one has to choose an ablation criteria. Several criteria has been proposed over time, the first one

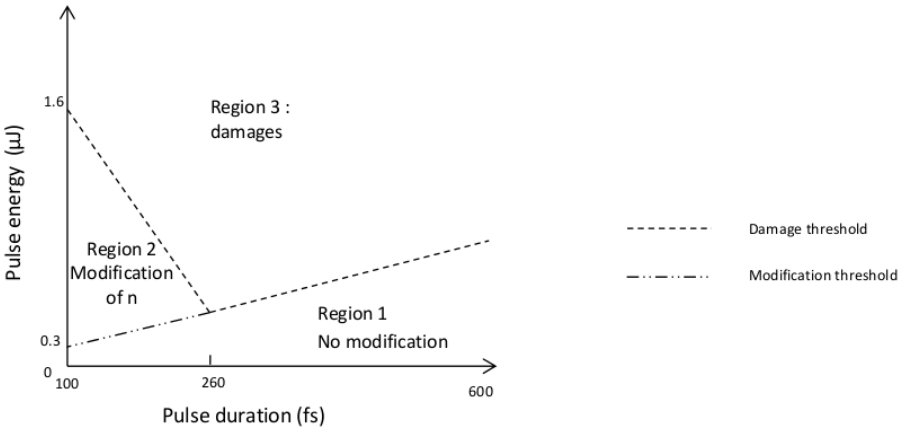

Figure 1.6: The different regimes : in region 1 no change are visible, in region 2 the refractive index is changed, in region 3 damages are visible.

being the intensity of the pulse, which has been contested due to the fact that it does not take into consideration the duration of the pulse[13]. A critical excitation density is often considered as the criteria from which ablation would occur, because it is thought that the depletion of the valence electrons would break bonds[7]. It has been criticized lately because it does not explain the molten matter often found on the periphery of the craters[20]. Coulomb explosion, that is to say coulombic repulsion between ions once the electrons responsible for bonds have been removed and a more energy related criteria has been proposed[21][22], explaining those thermal effects.

Chapter 2

The experiments

Our experiment is based on the principle of interferometry. We will present the basic idea of the experiment and the experimental setup that we used.

2.1 Pump-probe technique

The technique we have been using in all the experiments is the pump-probe technique. A first powerful pulse (aka the pump) is sent through the material first. Then a less powerful pulse (aka the probe) is sent at a certain delay after the pump. The pump, by exciting the electrons inside the material induces some transient modifications in the sample. For example, the reflection coefficient can change or the transmission through the sample of the pulse beam can be modified during all the time when the electrons are excited. This can be measured thanks to the probe pulse. Repeating the experiment with different time delays between the pump and the probe give the evolution of the electron density through a long time scale. The technique is illustrated in Fig.2.1.

In our case, we do not measure the reflection of the probe beam, because the met[23]hod is not sensitive enough, although there are plans to do it in the future. Instead, we measure the phase shift of the probe relative to a reference pulse, thanks to a method called frequential interferometry.

2.2 Frequential interferometry

2.2.1 Idea

In order to follow the dynamics of the electrons, we have to find a physical parameter that change following the density of excited electrons. This is the case of the refractive index (we will see later how the excitation of electrons can be accessed by the shift of the refractive index). The idea is to create interferences in the frequency domain thanks to two pulses delayed in time, in the same manner as two pulses with different frequencies can interfere in the

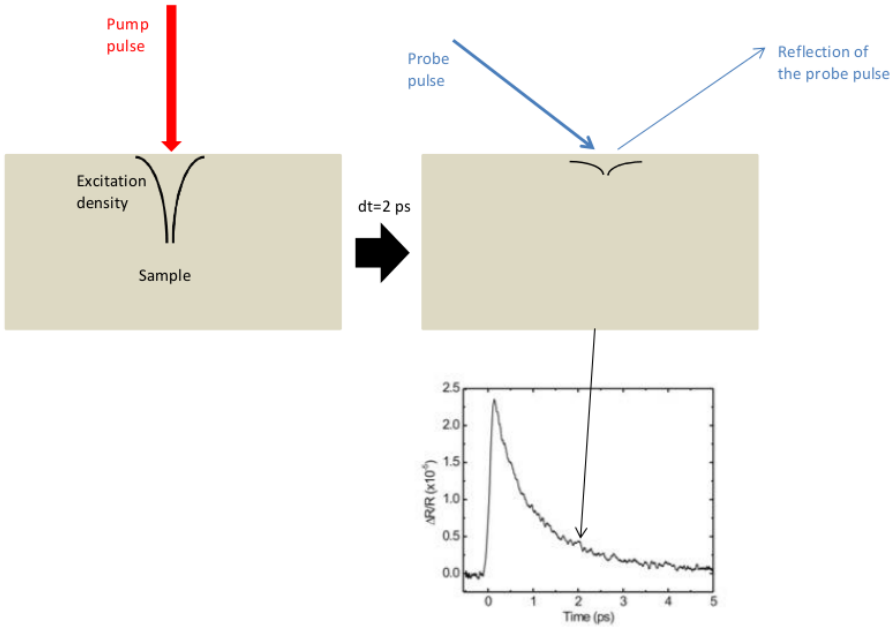

Figure 2.1: Example of an experiment with the pump-probe technique measuring the reflectivity of the beam

temporal domain and create beatings.The modifications of the refractive index is then accessible in the phase of the interferences. The reason why we are in the frequency domain is that spatial interferometry (such as the Young's double slit experiment) is not precise enough, because it is necessary to control very precisely the lengths of the two paths, which limits the measure of the phase shift. Here, the two pulses take the same path, so this is not a problem[24].

Experimentally, we use three pulses : one first probe pulse that "see" the material when the electrons are not excited and is so our reference pulse, one pump pulse that excites the medium, and a final probe that "see" the excited material. The two probe pulses interfere, and the phase of the resulting signal is measured. The measure is repeated for different time delays between the pump and the second probe, so that we can follow the dynamic of the excited electrons.

Let's write the electrical field of the reference probe :

$$E_1(t) = E_0 e^{i\omega_0 t}$$

If we suppose that the pump perturbs the medium before the second probe arrives, then the electrical field of the second probe is [23]:

$$E_2(t) = \sqrt{T} E_0(t - \Delta t) e^{i(\omega_0(t-\Delta t)+\Delta\phi)}$$

where T is the transmission factor and $\Delta\phi = \frac{2\pi L}{\lambda_{probe}}\Delta n$ is the phase shift induced by the pump and is related to the refractive index variation. If we look to the intensity in the frequency domain :

$$\tilde{I}(\omega) = \left|\tilde{E}(\omega)\right|^2 = \tilde{I}_0(\omega)\left[1 + T + \sqrt{T}cos(\Delta\phi - \omega\Delta t)\right]$$

where the $\tilde{}$ above the letters indicates the Fourier transform, $E = E_1 + E_2$, and $\tilde{I}_0(\omega) = \left|\tilde{E}_0(\omega - \omega_0)\right|^2$. $\tilde{I}$ is the actual physical value recorded by the CCD camera, the Fourier transform being done by a spectrometer. In order to obtain the physical response of the material, we have to know the phase of $\tilde{I}$. Let's write the inverse Fourier transform of $\tilde{I}$.

$$\mathrm{TF}^{-1}\left[\tilde{I}(\omega)\right] = (1+T)\,\mathrm{TF}^{-1}\left[\tilde{I}_0(\omega)\right] + 2\sqrt{T}\,\mathrm{TF}^{-1}\left[\tilde{I}_0(\omega)\right] \cdot \mathrm{TF}^{-1}\left[cos(\Delta\phi - \omega\Delta t)\right]$$

which we can rewrite :

$$\mathrm{TF}^{-1}\left[\tilde{I}_0(\omega)\right] = G_0(t) \text{ and } \mathrm{TF}^{-1}\left[\tilde{I}(\omega)\right] = G(t)$$

Thus :

$$G(t) = (1+T)G_0(t) + \sqrt{T}\left[G_0(t+\Delta t)e^{i\Delta\phi} + G_0(t-\Delta t)e^{-i\Delta\phi}\right]$$

If we suppose that the pulses are Gaussian , then :

$$G_0(t) = I_0 e^{-\frac{t^2}{\tau^2}} e^{i\omega_0 t}$$

Then :

$$G(t) = I_0 \Big\{ (1+T) e^{i\omega_0 t} e^{-t^2/\tau^2} + \sqrt{T} \left[e^{i\omega_0 (t+\Delta t)^2} e^{-(t+\Delta t)^2/\tau^2} e^{i\Delta\phi} + e^{-i\omega_0 (t-\Delta t)} e^{-(t-\Delta t)^2/\tau^2} e^{-i\Delta\phi} \right] \Big\}$$

If we measure G(t) for $t = \Delta t$, then :

$$G(\Delta t) = I_0 \left\{ (1+T) e^{i\omega_0 \Delta t} e^{-\Delta t^2/\tau^2} + \sqrt{T} \left[e^{-i\Delta\phi} + e^{i\omega_0 (2\Delta t)} e^{-(2\Delta t)^2/\tau^2} e^{i\Delta\phi} \right] \right\}$$

$$\text{i.e } \; G(\Delta t) \cong I_0 \sqrt{T} e^{-i\Delta\phi}$$

Thus, the phase of $G(\Delta t)$ gives us the phase shift $\Delta\phi$ and so the physical response of the material[23].

To sum up, we aim to measure the phase shift created by the pump. In order to do so, we use three pulses. The first one is the reference, the second the pump and the third the probe. The reference and the probe pulses interfere in the frequency domaine, and the interference created give the phase shift. In practical, the signal is recorded by a CCD camera, and the recorded area is large enough so that the area at the edge is not excited by the pump. This is possible because the radius of the probe is much larger than the pump one. Thus, we can use that unperturbed area as the reference, and so the reference pulse is not required. Instead, we use a michelson interferometer after the sample, with one branch slightly tilted, so that the two beams can interfere, in a way that the interference occurs between the edge of the probed area and the perturbed center. This is represented in Fig.2.2.

2.2.2 Experimental setup

The experiments have been made at the Saclay Laser-matter Interaction Center (SLIC: http://iramis.cea.fr/slic/index.php) facility. The laser is a CPA amplified Ti-Sa system, delivering up to 70mJ at 800nm, with a repetition rate of 20Hz. The experimental setup is shown in Fig.2.3. The laser beam is separeted in two by a beam splitter. The beam with most energy, the pump, can be frequency doubled by a BBO crystal. It goes through a controled delay line and is then focused on the sample. The other beam, the probe, goes through a controled delay line, and then through the sample. After that it is splitted in two pulses delayed in time thanks to a Michelson interferometer, Fourier transformed by the spectrometer and finally collected by a CCD camera.

2.2.3 The different contribution to the phase shift

It is possible to distinguish several contributions in the phase shift coming from different mechanisms : the main ones are the Kerr effect, the contribution from the free electrons, and the contribution from the trapped electrons.

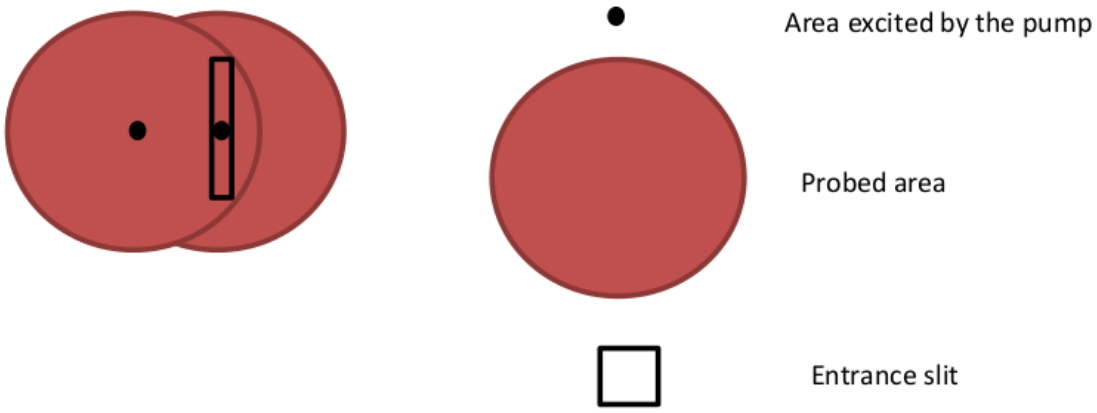

Figure 2.2: The two beams after the Michelson interferometer.

The Kerr effect

The Kerr effect arises in transparent media exposed to high intensities. It reflects the non-linearity of the refractive index under high intensities. In centrosymmetric crystals like ours, the second order polarization is absent. The next term is responsible for the Kerr effect. We can write the refractive index shift as [19] :

$$\Delta n = n_2 I_p$$

with $n_2$being the non-linear refractive index of the medium and I_p the intensity of the pump. The contribution of the Kerr effect is thus proportional to the intensity of the pulse, and it lasts as long. We can also note that the peak of the Kerr effect corresponds to the moment when the pump and the probe overlapped temporally, which is the $\Delta t = 0$ delay case.

Free electron model and contribution

This model gives the contribution of the electrons in the conduction bands, which we consider act freely, after they have been promoted there by the pump. The model uses the Drude model for free electrons. As we saw earlier, the complex refractive index of a solid in the free electron approximation is given by :

$$n^2(\omega_{probe}) = \epsilon_r = n_0^2 - \omega_{plasma}^2 \frac{f_{CB}}{\omega_{probe}^2 + i\omega_{probe}\omega_c}$$

with ϵ_r the relative permittivity, n_0 the unperturbed refractive index, f_{CB} the oscillator strength standing for transitions occurring in the conduction band

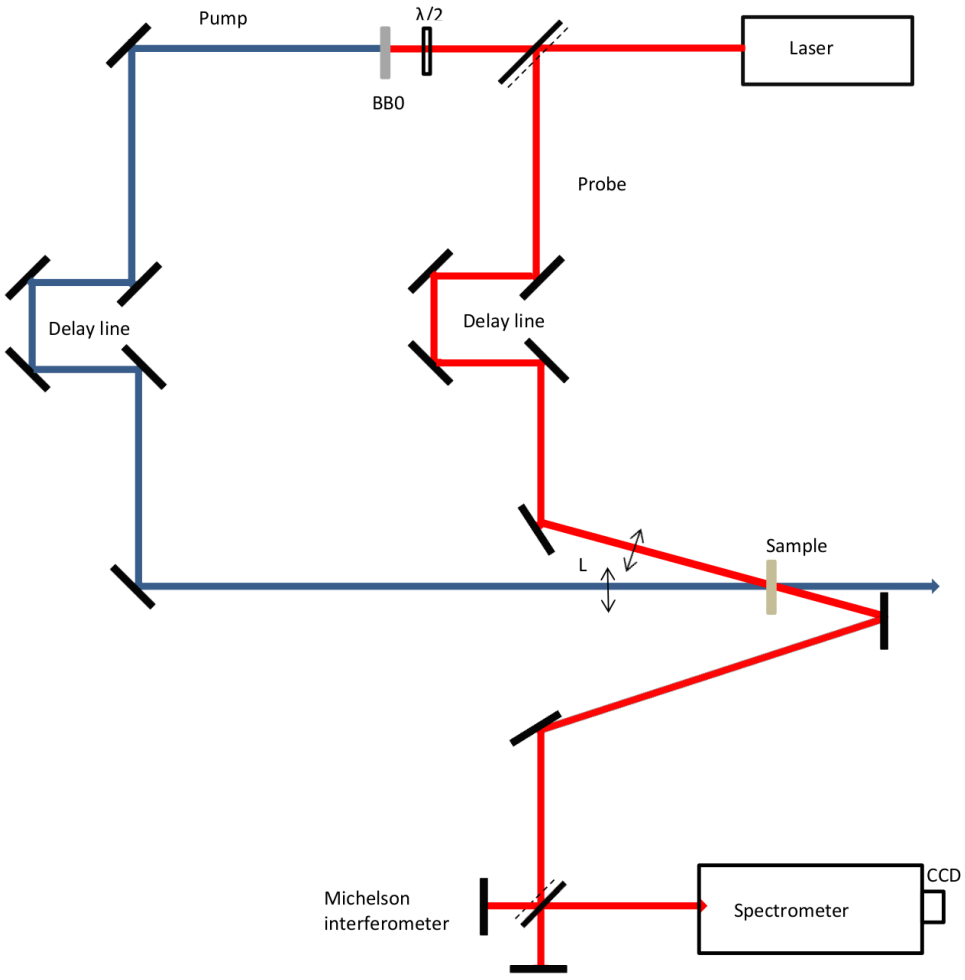

:

Figure 2.3: The simplified experimental setup

and ω_c being a damping term representing the probability of collisions between an electron and another electron, an ion or a phonon. ω_{plasma} is the plasma frequency and is given by :

$$\omega_{plasma} = \sqrt{\frac{Ne^2}{\epsilon_0 m*}}$$

where N is the density of excited electrons, e is the elementary charge, ϵ_0 is the vacuum permittivity, and m* is the effective mass.

Trapped electron model and contribution

In some materials such as in fused silica, a new contribution can be observed after the two first contributions (experimentaly around 150 fs). It corresponds to the trapping of the electrons in the conductive band. As we said previously, the electrons are trapped in induced defects called STE, which corresponds to the deformation of the lattice under high intensity. The contribution of the STE on the refractive index can be expressed as [25] :

$$n^2(\omega_{probe}) = \epsilon_r = n_0^2 - \omega_{STE}^2 \frac{f_{TR}}{\omega_{tr}^2 - \omega_{probe}^2 - i\omega_{probe}/\tau_{tr}}$$

with :

$$\omega_{STE} = \sqrt{\frac{N_{tr}e^2}{\epsilon_0 m_0}}$$

N_{tr} is the density of electrons trapped, m_0 is the mass of an electron, ω_{tr} is the energy difference between the fundamental and the first excited state of the induced defect, $1/\tau_{tr}$ is the width of this transition, and f_{tr} is the corresponding oscillator strength.

Valence band depletion

One minor contribution comes from the depletion of the valence band. If we consider a wide-bandgap being represented by a two level system, then :

$$n^2(\omega_{probe}) = \epsilon_r = 1 + \omega_{valence}^2 \frac{f_{12}}{\omega_{12}^2 - \omega_{probe}^2 + i\omega_{probe}/\tau_{12}}$$

with :

$$\omega_{valence} = \sqrt{\frac{N_v e^2}{\epsilon_0 m_0}}$$

N_0 is the density of electrons in the valence band, ω_{12} is the energy difference between the valence band and the conduction band, $1/\tau_{tr}$ is the width of this transition, and f_{tr} is the corresponding oscillator strength. We are far from resonance, (the energy of the incoming electrons equal to 9 eV whereas the resonance is around 1.5 eV), so the damping term can be neglected. Thus, $n^2(\omega_{probe}) = n_0^2$.

This relation is correct when the dielectric is in its fundamental state, but is no longer true when electrons leave the valence band and go to the conduction band, or are trapped. Instead, we should write :

$$\omega_{valence,depl} = \sqrt{\frac{(N_v - N - N_{tr})e^2}{\epsilon_0 m_0}}$$

In this case, we can write :

$$n^2(\omega_{probe}) = with \epsilon_r = 1 + \omega^2_{valence,depl} \frac{f_{12}}{\omega^2_{12} - \omega^2_{probe} + i\omega_{probe}/\tau_{12}}$$

2.2.4 Conclusion

To sum up, we can rewrite the refractive index, taking into account all the different contributions [25]:

$$\begin{aligned} n^2(\omega_{probe}) =& 1 + \frac{e^2}{m\epsilon_0}(N_v - N - N_{tr}) \frac{f_{12}}{\omega^2_{12} - \omega^2_{probe} - i\omega/\tau_{12}} + \chi^{(3)} I \\ &+ \frac{e^2}{\epsilon_0}(-\frac{N\, f_{CB}}{m*} \frac{1}{\omega^2_{probe} + i\omega_{probe}\omega_c} + \frac{N_{tr} f_{tr}}{m_0} \frac{1}{\omega_{tr} - \omega^2_{probe} - i\omega_{probe}/\tau_{tr}}) \end{aligned}$$

The phase shift is then calculated as :

$$\Delta\phi = \frac{2\pi}{\lambda_{probe}} \left[\int_0^L \mathrm{Re}(n(z) - n_0) dz \right]$$

where L is the length along which the probe and the pulse overlap. If we suppose that the densities of the excited electrons and of the trapped electrons are small compared to the valence density, and that the damping terms can be neglected, then it is possible to have an approximate expression of $\Delta\phi$ [25]:

$$\Delta\phi \approx \frac{2\pi}{\lambda} L \left[n_2 I_p + \frac{e^2}{2n_0\varepsilon_0} \left\{ -\frac{N\, f_{CB}}{m * \omega^2} + \frac{N_{tr} f_{tr}}{m(\omega^2_{tr} - \omega^2)} \right\} \right]$$

Although rather crude, the approximations make it possible to clearly see the different contributions : the first term is the Kerr effect proportional to the intensity of the pump which contributes positively to the phase shift because n_2 is positive. The second term is the contribution of the free electrons, always negative, and the last term is the contribution of the trapped electrons, whose sign depends on the values of ω_{tr} and ω. In our experiment, $\omega < \omega_{tr}$, so this contribution is positive.

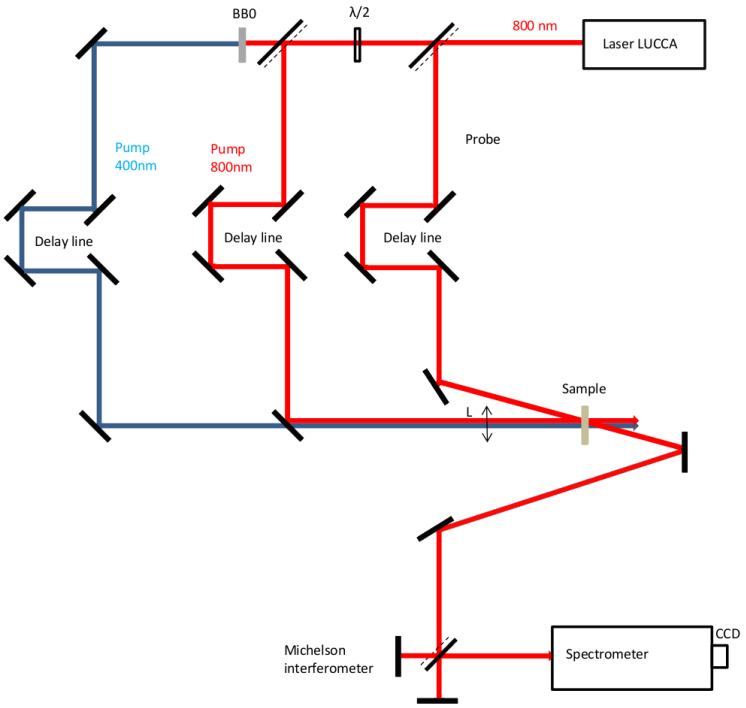

Figure 2.4: Two pumps experimental setup

2.3 Two pumps experiment

Recently, new experiments using two pumps has been created, both for fondamental purpose [24] and for more applied purpose, like laser machining [26].

In our group, we use two pumps in order to separate the contributions of the different mecanisms : the idea was to use the first UV pump pulse to promote the electrons from the valence band to the conduction band, and the second IR pump pulse to heat the electron already in the conduction band via inverse Bremsstrahlung, and trigger electronic avalanche. This way, the two main mechanims are clearly associated to one pulse : multiphoton absorption with the UV pulse, and electronic avalanche with the IR pulse [24].

The setup is mostly the same as the single pump pulse, the difference being that after being splitted by the beam splitter, the powerful beam is even more splitted. The two newly created beams are the two pumps, one is frequency doubled by a BBO crystal, and the other keeps its frequency. The duration of the pulses can be controled. Then both of them are fired on the sample. This is illustrated in Fig.2.4

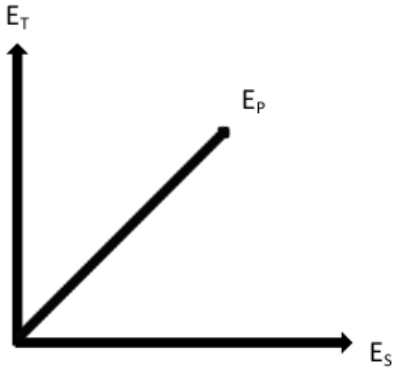

Figure 2.5: Polarizations configuration

2.4 Transmission measure

2.4.1 Idea

As we will see in the results of this experiment, it seems like in some case we have to take into account the fact that phonons are also excited by the laser and can perturb our results. In order to conclude whether or not the phonon are excited, we decided to do an experiment solely on phonons in order to compare it with our data. This experiment was done in the Laboratoire d'Optique Appliquée (LOA) in Palaiseau.

A coherent phonon in a crystal has for consequences a change in the refractive index and the creation of an emitted field. The easiest way of detecting the phonon is to measure the emitted field it created. It can be shown ([27]) that the emitted field is equal in the frequency domain to :

$$E_S(\omega, z) = \left(\frac{\pi\omega z Q_0}{n\,c}\right)\left(\frac{\partial\chi^{(3)}}{\partial Q}\right)_0 \left[e^{i\omega_0\tau_D}E_T(\omega+\omega_0) - e^{-i\omega_0\tau_D}E_T(\omega-\omega_0)\right]$$

where $\omega = \omega_p + \omega_L$ (with ω_L the frequency of the probe and ω_p the frequency of the pump taken to be equal to ω_0 the frequency of the Raman mode), Q_0 the amplitude of the phonon, $\chi^{(3)}$ the third order susceptibility, τ_D the delay between the pump and the probe and E_T the probe field. We also have to consider the polarization of the pulses. Here we take the probe polarizations to be 45 degrees with respect with the pump. In this configuration, the emitted field polarisation is orthogonal with the probe (cf. Fig.2.5).

Two types of measures are then possible [27] : the homodyne detection, which measure the square of the emitted field, and the heterodyne detection, which measures the field linearly. Both implies the use of a analysor in order to discriminate the emitted field from the two others, using its polarization. The

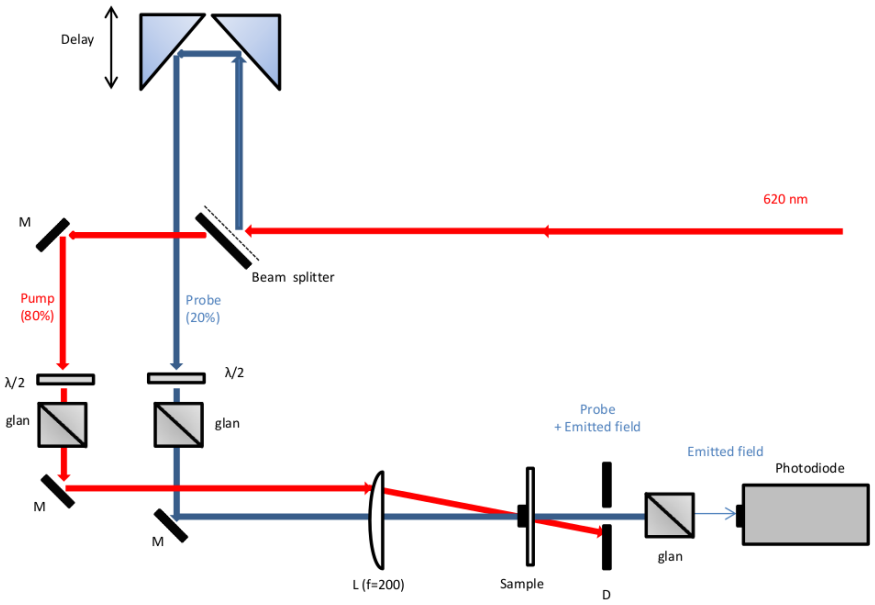

Figure 2.6: Experimental Setup

homodyne detection is really just the measure of the intensity of the emitted field.

The heterodyne detection is better experimentaly because the emitted field contribution is amplified by the interference term from a local oscillator. Experimentaly, this is done by polirizing slightly the probe field so that there is a small component of the probe in the direction of the emitted field. Mathematically :

$$I_H = \frac{nc}{8\pi} |E_{LO} + E_S|^2 = \frac{nc}{8\pi} \left(|E_{LO}|^2 + |E_S|^2 + E_{LO}E_S^* + E_{LO}E_S^* \right)$$

For a Gaussian beam, in the time domain, we have :

$$E_T(t) = Ae^{-(t^2/(2\tau_L^2))} e^{i(k_L z - \omega_L t)}$$

and :

$$E_{LO}(t) = \alpha e^{-(t^2/(2\tau_L^2))} e^{i(k_L z - \omega_L t)} e^{i\varphi}$$

2.4.2 Experimental setup

The experimental setup is represented in Fig.2.6; the main difference with the previous setup is the poralizer before the photodiode. The pump wavelength was 800 nm, the radius of the probe 40 µm and the radius of the probe 40 µm.

Chapter 3

Experimental results

3.1 Frequential interferometry

3.1.1 Single pump pulse experiment

3.1.1.1 Short time scale

The experiment with one pump gives the kind of figures presented in Fig.3.1, showing the evolution of the phase shift over time in SiO_2 [25]. Those evolutions can be linked to the different phenomena we presented before. When the signal is equal to zero, that means that the probe comes before the arrival of the pump, thus giving no signal. The positive phase shift at 0 is the Kerr effect. Its maximum corresponds to the time when the pump and the probe overlap perfectly in time. The next negative contribution is the contribution of the free electrons in the conduction band. Finally, the signal rises again to a positive value. That is the contribution of the STE.

This experiment has been done for several pulse energy, the reults are shown in Fig.3.2. Althought the curves are not perfect (not a lot of signal, lot of absorption because of pulse energy too important), what can be seen is that the more powerful the pulse is, the more the phase shift is imporant. This is because more electrons are promoted to the conduction band. This experiment has been repeated for several materials. The results in Al_2O_3 are shown in fig3.3. As one can see, other materials give different results. In particular, the signal does not go above zero after the negative contribution in Al_2O_3, meaning that there is no STE. Instead, the electrons only relaxe by scattering processes. If we increase the intensity of the light, the negative contribution goes lower and lower, again because more and more electrons are excited (Fig.3.4).

An interesting result in Fig.3.1 is the very small oscillations that can be seen when the signal goes positive again. We believe that this comes from the excitation of the phonons in the material, and this is the reason why we decided to do a specific experiment on phonons .

Those results show very well the dynamics of the electrons in the femtosecond

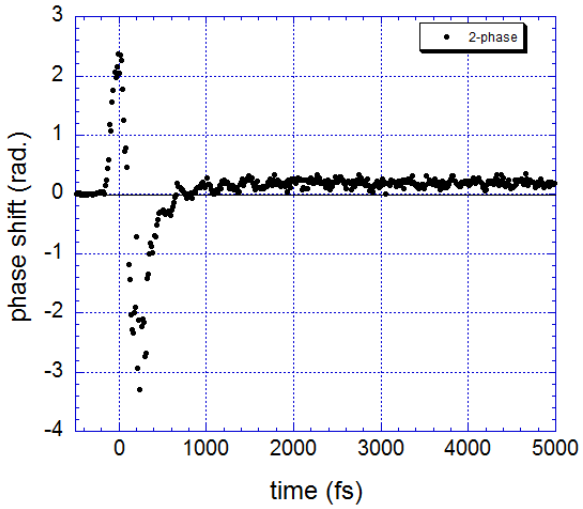

Figure 3.1: Phase shift in SiO_2 for a laser pulse of 230 µJ, $\lambda = 800$nm

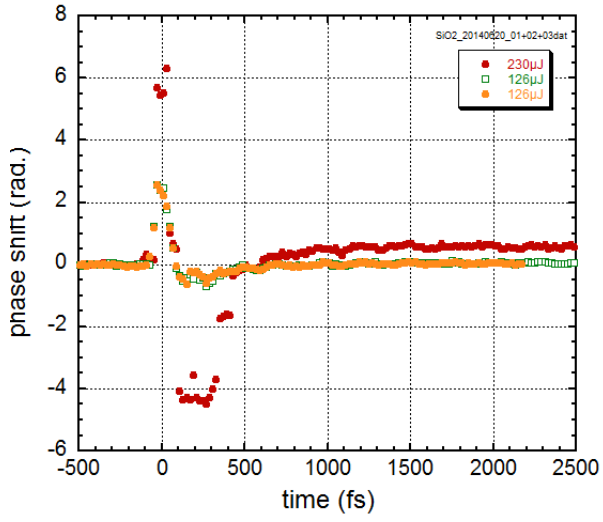

Figure 3.2: Phase shift in SiO_2 for different pulse energies

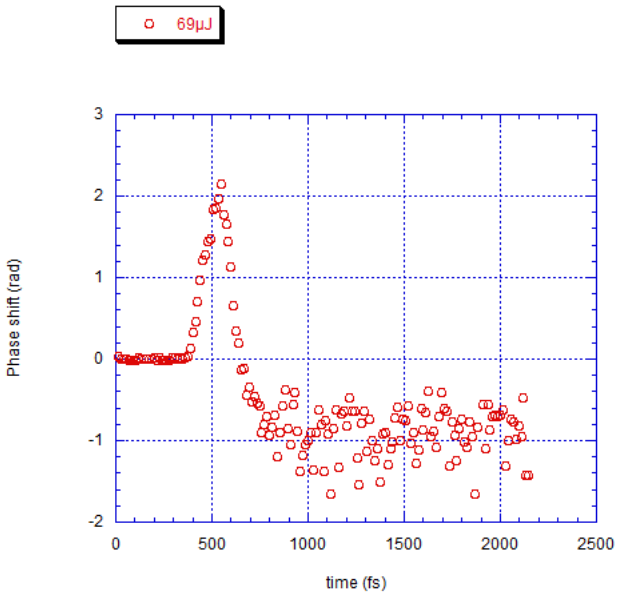

Figure 3.3: Phase shift in Al_2O_3 for a laser pulse of 230 µJ, $\lambda = 800$nm

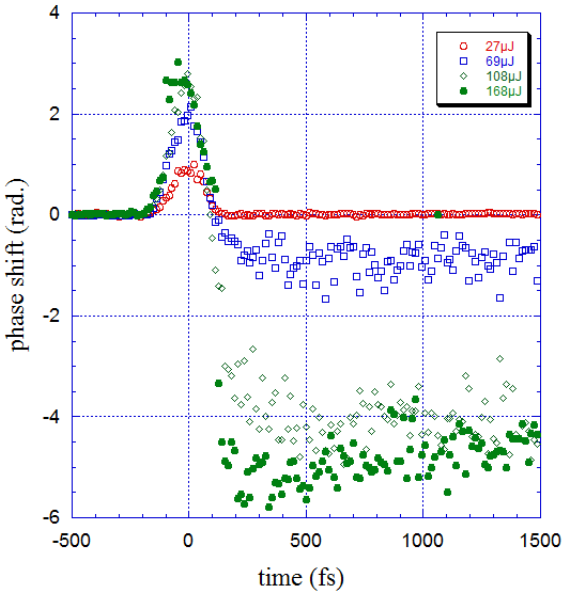

Figure 3.4: Phase shift in Al_2O_3 for different pulse energies

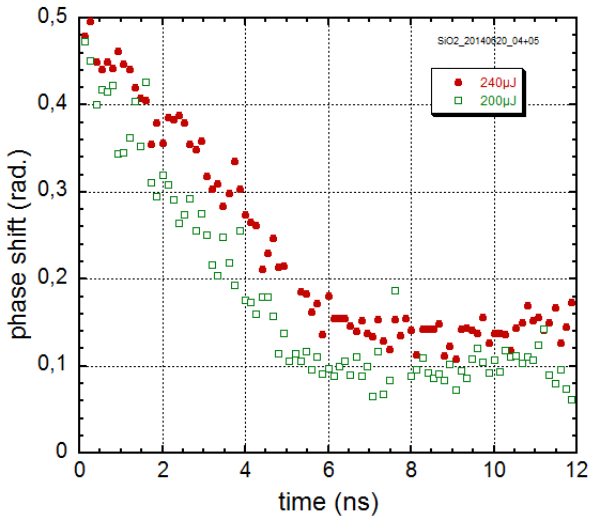

Figure 3.5: Phase shift in the nanosecond regime for two pulse energies.

regime. It would also had been interesting to follow the relaxation over time, but previous studies has shown that the STE lifetime, never measured precisely, was longer that one nanosecond. Our experiment could not go that far, because of the limited lenght of the delay line. This was the motivation for a modification of the experimental setup.

3.1.1.2 Long time scale

We focus in this section to SiO_2. We measured the relaxation of the STE on a large time scale, up to 10 ns. We were able to do so by adding a very long delay line in the setup for the probe pulse (delay line of 2 meters long, operated by hand). The result is ploted in Fig.3.5. It enabled us to measure its lifetime : 6 ns. As can be seen, this results is consistent for the two pulse energies. Interestingly, the phase shift at the end in not equal to 0, but is still positive. This is still to be studied.

3.1.2 Two pump pulses experiment

We have two reasons to use two pumps. First, it will make the separation of the two main mechansims easier to see : the UV pump excites the electrons from the valence band to the conduction band purely by multiphoton absorption (because it only takes 3 photons for UV pulse to promotes electrons in the conduction band instead of 6 for the IR pulse, it is far more efficient), and the IR pump pulse heats the electrons in the conduction band in order to trigger impact ionisation (which is made possible because the cross section for heating is bigger for IR

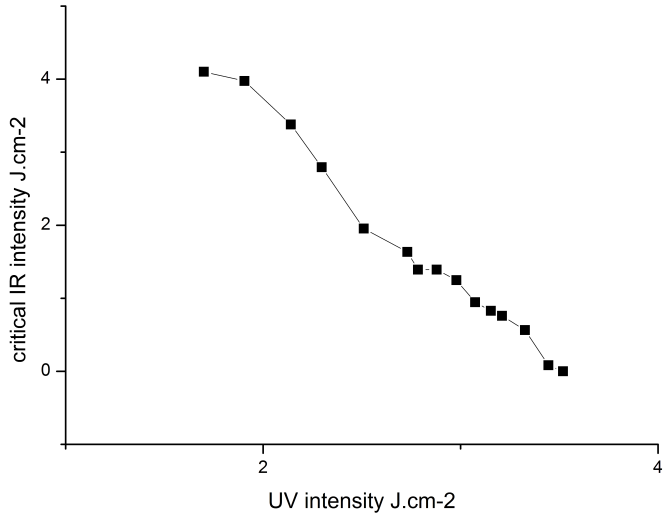

Figure 3.6: Intensities at damage threshold in Al_2O_3 for a 300fs IR pulse as a function of a 60fs UV pulse. The delay between the two pulses is fixed at 936 fs.

than for UV, making it more efficient for the IR pulse). Secondly, it makes possible to discuss the ablation criteria. It is generally accepted that it is the excitation density that determines the presence of ablation, but as we will see, it might not always be true because in some case it is possible for the same density to lead either to ablation and not to ablation.

3.1.2.1 Intensities at damage treshold experiments

The first experiment that has been done is the measure of the critical IR pump pulse intensity as a function of the UV pump pulse intensity from which damages can be seen in the sample. The delay between the two pump pulses was fixed to 936 fs in Al_2O_3 and 1.75 ps in SiO_2. This was done so that when the IR pulse arrives, the medium is already pre-excited by the UV-pulse, and in SiO_2 the STE are already trapped. The result can be seen in Fig.3.6 and Fig.3.7 [24]. We will use those experiement later.

3.1.2.2 Phase shift experiments

By measuring the phase shift created by the sequence of 2 pulses UV and IR, and by comparing it to single pulse phase shift, it has been proved by a previous PhD student that no impact ionisation occurs in Al_2O_3, contrary to SiO_2 [24]. The reason why the situation is different for the two materials is still unclear.

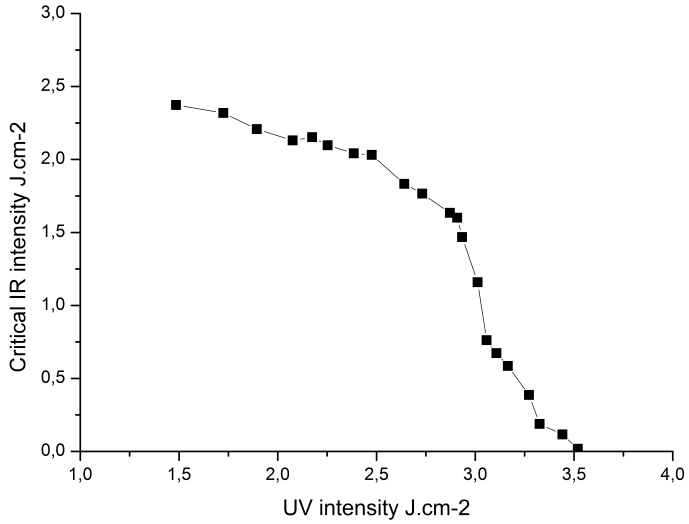

Figure 3.7: Intensities at damage threshold in SiO_2 for a 300fs IR pulse as a function of a 60fs UV pulse. The delay between the two pulses is fixed at 1.75 ps.

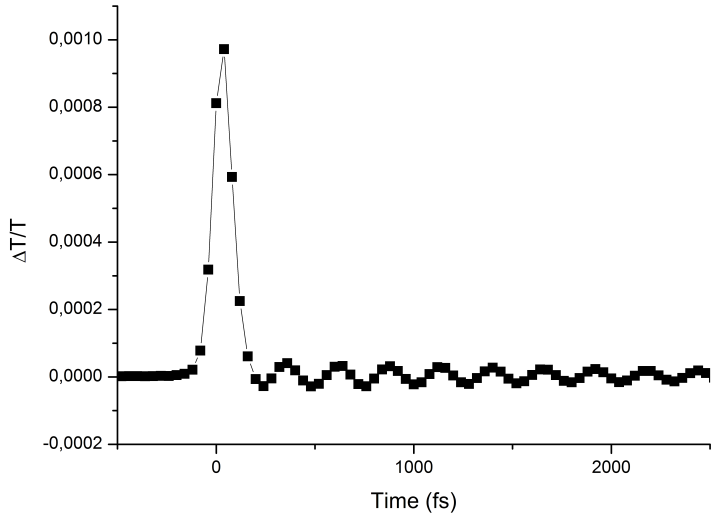

Figure 3.8: Pump-probe measurement on SiO_2 in heterodyne configuration

One hypothesis would that the ionization cross section is material dependent, but again, there is no clear reason why that would be the case.

3.2 Transmissions measures

In the heterodyne configuration, the results of our experiment can be see in Fig.3.8. The first peak is the Kerr effect, and the following dumped oscillations are due to the phonons. The period of oscillations is 260fs. From these experiments, it is also possible to calculate the displacement of the phonons [27].

Chapter 4

Exploitation of the results

The major part of the thesis was the numerical simulation of all the phenomena. First we had to simulate the propagation of the pulse inside the material taking into account all the mechanisms that occur as the pulse propagates. Then, using this simulation we were able to reproduce the experimental results, and to calculate the absorbed energy.

4.1 The propagation algorithms

4.1.1 Single pulse rate equations

The aim is to calculate the temporal and spatial evolution of the excited carrier density N and the photon flux of the exciting pulse, F.

For Al_2O_3 :

Let's describe the model we have been using in order to simulate the propagation of the laser pulse inside Al_2O_3 [25]:

$$\begin{aligned}\frac{\partial N}{\partial t} =&(N_{tot} - N)\sigma_n F^n \\ \frac{\partial F}{\partial y} =&- n(N_{tot} - N)\sigma_n F^n - \alpha F\end{aligned}$$

Where n is the order of the multiphoton process,τ is the electron trapping time, $F = \frac{I}{\omega\hbar}$ is the fluence of the pump and $\alpha = 2\omega \mathrm{Im}(\sqrt{\varepsilon_r})/c$ is the absorption coefficient due to the plasma at the surface of the sample. The first equation shows the evolution of N over time ; the term on the right is the excitation due to multiphotonic absorption. The last equation shows the evolution of F_p over depth ; the first term is related to the multiphoton absorption, and the last term represents the absorption due to the plasma.

As can be seen, there is no impact ionization, because as we have seen previsously, it seems there is no impact ionization into Al_2O_3. It is also worth

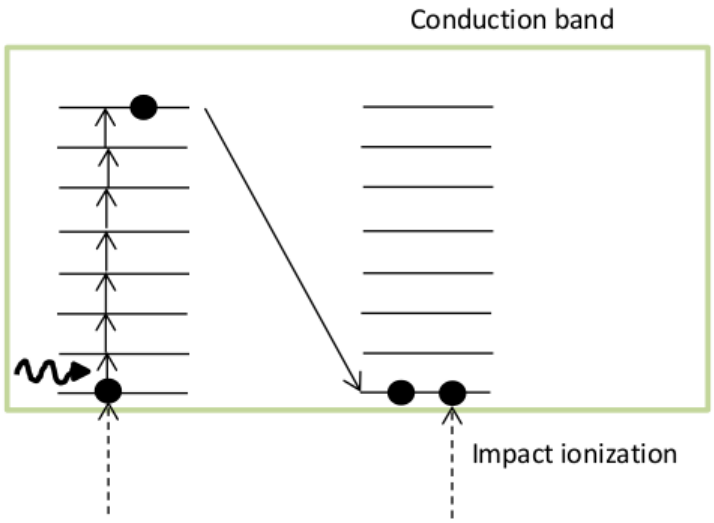

Figure 4.1: Descritization of the conduction band

noticing that heating of the excited electrons inside the conduction band is not simulated neither. Because there is no impact ionization, this does not have any effect on the density of electrons, but as we try to calculate the amount of energy absorbed, it will be necessary to use a trick to reproduce the amount of energy heating would have absorbed.

For SiO_2 :

In SiO_2, it is now important to modelise the possible heating of the electrons in the bottom of the conduction band. This is done by descritizing the energies of the electrons inside the conduction band and assuming the transitions are possible for one photon absorption [28] (see Fig.4.1).

This allows us to introduce impact ionization. This was done using the results in [7]. We also have to simulate the trapping of electrons.

Overall, the new equations give for two levels of energy inside the conduction band :

$$
\begin{aligned}
\frac{\partial N_1}{\partial t} &= N_v \sigma_n F^n + 2\Gamma_2 N_2 F - \beta N_1 F - N_1/\tau \\
\frac{\partial N_2}{\partial t} &= \beta N_1 F - \Gamma_2 N_2 F - \frac{N_2}{\tau} \\
\frac{\partial N_{tr}}{\partial t} &= N_1/\tau + N_2/\tau \\
N_v &= N_{tot} - N_1 - N_2 - N_{tr} - \Gamma_2 N_2 \\
\frac{\partial F}{\partial y} &= -nN_v \sigma_n F^n - \alpha F
\end{aligned}
$$

Where n is the order of the multiphoton process, N_1, N_2 and N_v are respectively the density of electrons in the bottom of the conduction band, in the second level of energy in the conduction band, and in the valence band, N_{tr} is the density of trapped electrons,τ is the electron trapping time, $F = \frac{I}{\omega\hbar}$ is the fluence of the pump, $\alpha = 2\omega \mathrm{Im}(\sqrt{\varepsilon_r})/c$ is the absorption coefficient due to the plasma at the surface of the sample, β the cross section for 1 photon, and Γ_2 the impact ionization coefficient of the second level. . The first equation shows the evolution of N_1 over time ; the first term is due to the multiphoton absorption, the second to impact ionization, the third represents the heating of electrons to the second level of energy inside the conduction band, and the second term represents the trapping of the electrons. The first term in the second equation which represents the evolution of N_2 over time is the heating from N_1, the second represent impact ionization, and the last the trapping . There is no way to solve analytically those coupled partial differential equations, so we had to use a numerical method.

It is worth noticing that for neither Al_2O_3 nor SiO_2 did we simulate the relaxation of electrons. This is simply because we are focused on short time scale.

Now, let's take a look on how those coupled equations were numericaly resolved.

4.1.2 The finite difference method

The basic idea behind the finite difference method is to use the Taylor development in order to approximate the partial derivative.

From the definition of the derivative, we can write :

$$\frac{\partial f(x,y)}{\partial x} = \lim_{h_x \to 0} \frac{f(x+h_x, y) - f(x,y)}{h_x}$$

If $h_x \ll 1$, the Taylor development of $f(x+h_x, y)$ gives

$$f(x+h_x, y) - f(x,y) + h_x \frac{\partial f}{\partial x} + \theta(h_x) \simeq f(x,y) + h_x \frac{\partial f}{\partial x}$$

So :

$$\frac{\partial f(x,y)}{\partial x} \simeq \frac{f(x+h_x, y) - f(x,y)}{h_x}$$

We can then rewrite our Al_2O_3 equations in that manner, and resolve them. The newly written equations read :

$$\begin{aligned}\frac{N(y,t+dt)-N(y,t)}{h_t} &= (N_{tot}-N(y,t))\sigma_n F^n(y,t)\\ \frac{F(y+dy,t)-F(y,t)}{h_y} &= -n(N_{tot}-N(y,t))\sigma_n F^n(y,t)-\alpha(y,t)F_p(y,t)\end{aligned}$$

that is to say :

$$\begin{aligned}N(y,t+dt) &= h_t(N_{tot}-N(y,t))\sigma_n F^n(y,t)+N(y,t)\\ F(y+dy,t) &= -nh_y(N_{tot}-N(y,t))\sigma_n F^n(y,t)-h_y\alpha(y,t)F_p(y,t)+F(y,t)\end{aligned}$$

where we see that the different values are calculated for a certain number of points. Thus, we have to carefully choose a mesh, where the point will be calculated.

4.1.3 The 1D algorithm

We used the finite difference method in order to solve the rate equations.

Here is the algorithm we used, in the matlab language, for solving the rate equations in 1D in Al_2O_3:

```
for i0=1:nt-1
        for j=1:ny-1

                N(i0+1,j)=ht*sigma*(u-N(i0,j))*F(i0,j)^n+N(i0,j);

                n00(i0+1,j)=1+(ee^2/(2*m*epsilon0))*(u-Ntr(i0+1,j)-N(i0
                    +1,j))*f12/(w12^2-w^2);

                epsilonr(i0+1,j)=n00(i0+1,j)+F(i0+1,j)*h*w*chi3+(ee^2/
                    epsilon0)*(-N(i0+1,j)*fcb/(m*(w^2+1i*w/tauep)));

                alpha(i0+1,j)=imag(sqrt(epsilonr(i0+1,j)))*2*w/c;

                F(i0,j+1)=F(i0,j)*(1-hz*alpha(i0,j))-hy*sigma*n*(u-N(i0,
                    j))*F(i0,j)^n;

        end
end
```

The mesh we choose was such that the depth probed (that is to say 1µm) was divided into 500 points. The time scales from 0 to 1 ps by 10 fs step.

The algorithm gives us each parameters among depth (y) and time (s). For example, in Fig.4.2, the intensity of the pump is given along the depth y and the time t.

The phase shift is then calculated by :

```
for j0=1:ny
        DeltaPhi1(1,j0)=trapz(z,(2*pi/lambda)*(real(sqrt(epsilon2(j0,:))
            )-n0));
end
```

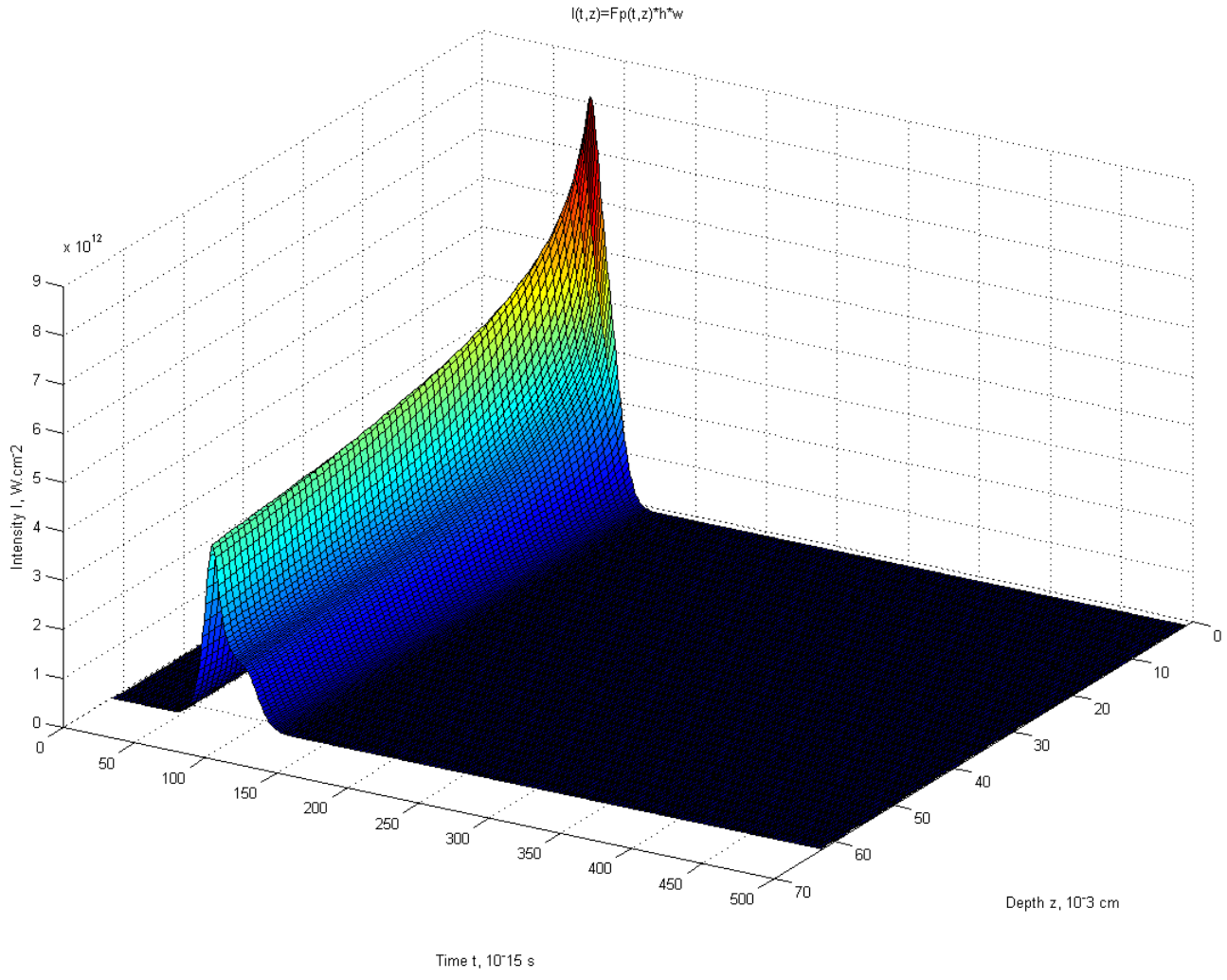

Figure 4.2: I(t,z)

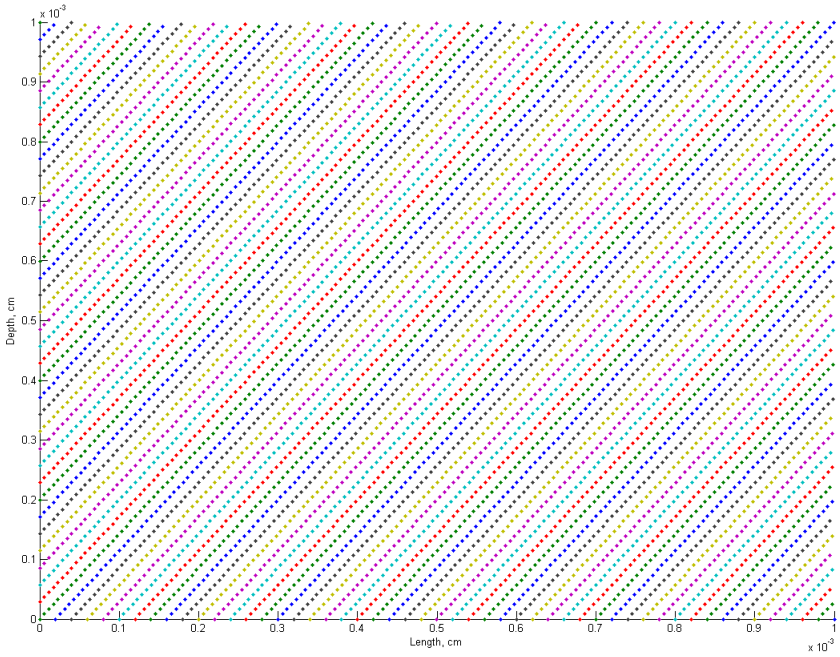

Figure 4.3: Example of a mesh for $\theta = 35^{\circ}$

Although sufficient in some case, this algorithm is restricted : it solves the rate equations only in one dimension, and there is no way to choose the geometry of the experiment, such as the incoming angle of the probe or the pump with respect to the surface, or the actual position of the probe. In order to do that, we have to solve the rate equations in 2D.

4.1.4 The 2D algorithm

All the code used in order to create the graphs is displayed in annex A.

The first thing we need to do is create the mesh. The points constituting the mesh were chosen in order to facilitate the calculus : the idea was to use the 1D algorithm along the choosen direction, the points on which the algorithm is to be applied being chosen so that they are aligned along the direction of propagation of the pump. In this way, we can choose freely the angle of incidence of the pump. The result can be seen Fig.4.3.

Then we apply the 1D algorithm rewritten for this configuration over each of the lines of points. The result can be seen Fig.4.4:

We can freely choose the characteristics of the probe, that is to say the position of its center, its radius, and the angle it makes with respect to the

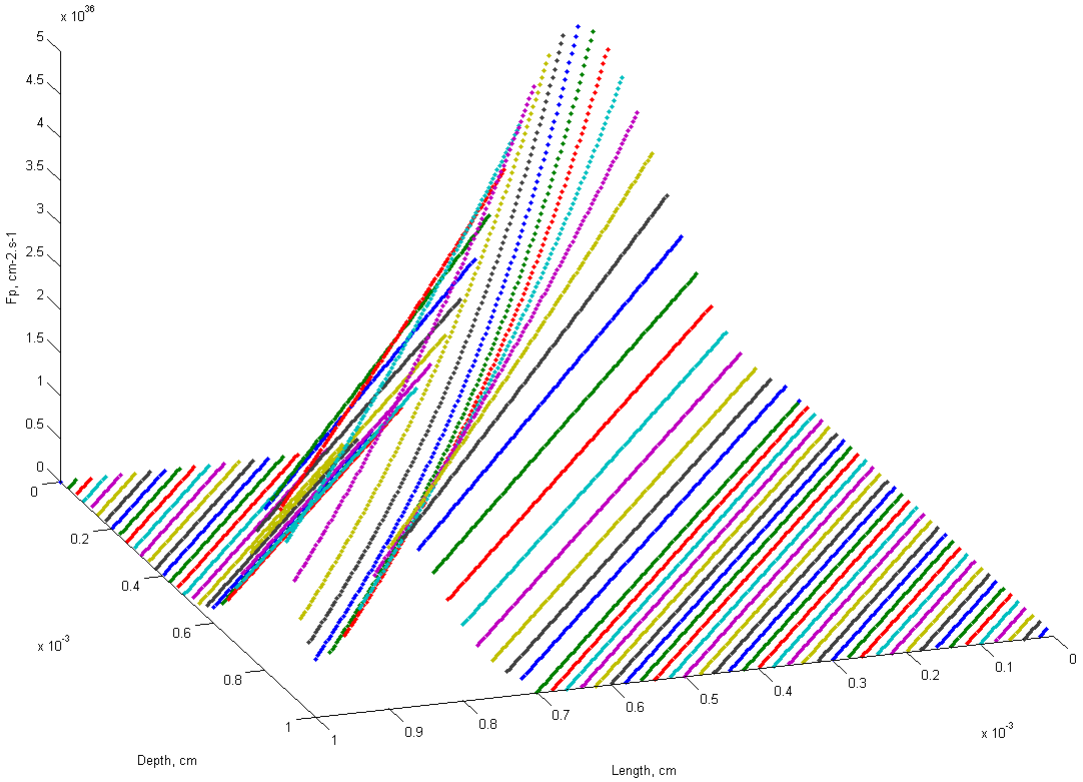

Figure 4.4: F_p at $t = 5.7 \cdot 10^{-13}$, for $\theta = 35^\circ$ and FMHW=150fs

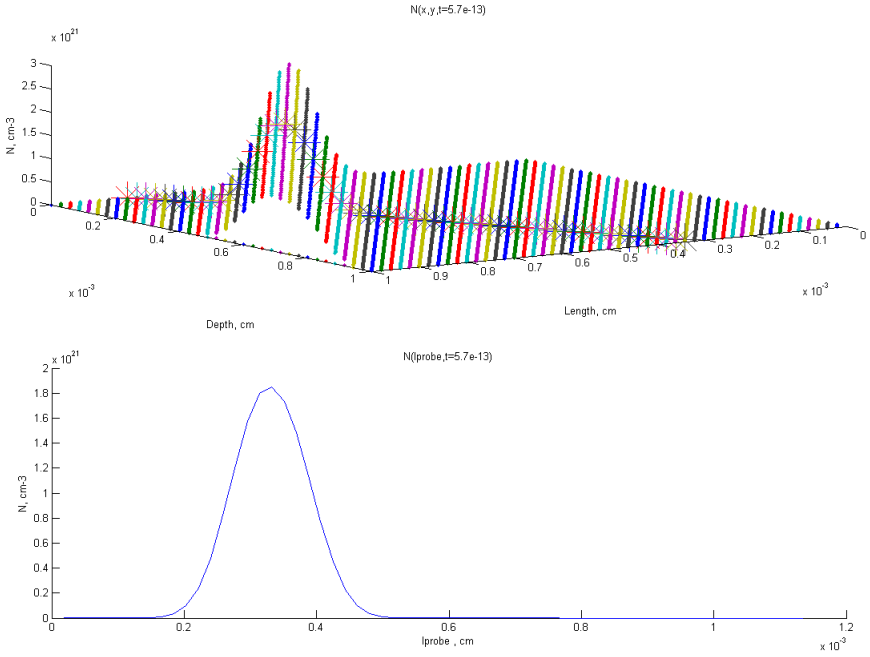

Figure 4.5: Density of excitation and probe at $t = 5.7 \cdot 10^{-13}$

sample surface. This is shown in Fig.4.5. The stars in the top graph correspond to the propagation of the center of the probe. The bottom graph reprents the excitation density of the material along the path of the center of the probe. This is shown in Fig.4.5. The stars in the top graph correspond to the propagation of the center of the probe. The bottom graph reprents the excitation density of the material along the path of the center of the probe.

From that point, we can then calculate the phase shift. We now have the possibility to calculate more precise simulations. This will come handy in the following.

4.1.5 Two pump pulses algorithm

In Al_2O_3 :

With two pump pulses, the equations are a little bit more complicated.

$$
\begin{aligned}
\frac{\partial N_1}{\partial t} =& N_v \sigma_{n_1} F_1^{n_1} + N_v \sigma_{n_2} F_2^{n_2} \\
N_v =& N_{tot} - N_1 \\
\frac{\partial F_1}{\partial y} =& - n_1 N_v \sigma_{n_1} F_1^{n_1} - \alpha F_1 \\
\frac{\partial F_2}{\partial y} =& - n_2 N_v \sigma_{n_2} F_2^{n_2} - \alpha F_2
\end{aligned}
$$

In SiO_2 :

We have to consider the reexcitation of the trapped electrons to the conduction band. In general, one level of energy in the conduction band is described as :

$$
\begin{aligned}
\frac{\partial N_i(z,t)}{\partial t} =& \beta_{i,1} N_{i-1}(z,t) F_1(z,t) + \beta_{i,2} N_{i-1}(z,t) F_2(z,t) - \beta_{i+1,1} N_i(z,t) F_1(z,t) \\
& - \beta_{i+1,2} N_i(z,t) F_2(z,t) - \frac{N_i(z,t)}{\tau} - \Gamma_i N_i(z,t)
\end{aligned}
$$

with $\beta_{i,1}$ and $\beta_{i,2}$ being the cross section for 1 photon at the level i, τ being the life time of the electrons on the level before being trapped, and Γ_i the impact ionization coefficient for the ith level.

Overall, the new equations give for i=2 :

$$
\begin{aligned}
\frac{\partial N_1}{\partial t} =& N_v \sigma_{n_1} F_1^{n_1} + N_v \sigma_{n_2} F_2^{n_2} - N_1/\tau - \beta_1 N_1 F_1 - \beta_2 N_1 F_2 + 2\Gamma_2 N_2 F_2 + 2\sigma_{n_3} N_{tr} F_2^{n_3} \\
\frac{\partial N_2}{\partial t} =& \beta_1 N_1 F_1 + \beta_2 N_1 F_2 - \frac{N_2}{\tau} - \Gamma_2 N_2 F_2 \\
\frac{\partial N_{tr}}{\partial t} =& N_1/\tau + N_2/\tau - 2\sigma_{n_3} N_{tr} F_2^{n_3} \\
\frac{\partial N_v}{\partial t} =& N_{tot} - N_1 - N_2 - N_{tr} - \Gamma_2 N_2 F_2 \\
\frac{\partial F_1}{\partial y} =& - n_1 N_v \sigma_{n_1} F_1^{n_1} - \alpha F_1 \\
\frac{\partial F_2}{\partial y} =& - n_2 N_v \sigma_{n_2} F_2^{n_2} - \alpha F_2
\end{aligned}
$$

Again, we use the finite difference method in order to resolve thoses equations numerically.

4.1.6 Calculus of the deposited energy

In Al_2O_3 :

If we consider two levels of energy in the conduction band, the deposited energy is calculated as [12]:

$$E_{abs} = \int_t \iiint_V (\frac{2\omega_1}{c} F_1 \hbar\omega_1 \mathrm{Im}(\sqrt{\varepsilon_2}) + \frac{2\omega_2}{c} F_2 \hbar\omega_2 \mathrm{Im}(\sqrt{\varepsilon_2}) + n_1\sigma_{n_1}F_1^{n_1} + n_2\sigma_{n_2}F_2^{n_2}) dV dt$$

The first two terms are the amount of energy absorbed by the plasma formed at the surface of the sample. The next two terms represent the amount of energy absorbed for the heating of the electrons. The expression is integrated over time and volume. As can be seen, even though we do not have a second level on energy, we can still calculate the amount of energy absorbed by the heating of electrons.

In SiO_2 :
If we consider two levels of energy in the conduction band, the deposited energy is calculated as :

$$E_{abs} = \int_t \iiint_V (\frac{2\omega_1}{c} F_1 \hbar\omega_1 \mathrm{Im}(\sqrt{\varepsilon_2}) + \frac{2\omega_2}{c} F_2 \hbar\omega_2 \mathrm{Im}(\sqrt{\varepsilon_2}) + n_1\sigma_{n_1}F_1^{n_1} + n_2\sigma_{n_2}F_2^{n_2} + 2n_3\sigma_3 F_2^{n_3}) dV dt$$

The only difference compared to Al_2O_3 is that we consider the reexcitation of the trapped electrons. The expression is integrated over time and volume.

4.2 Results for Al_2O_3

4.2.1 Phase simulation

In table 1 is written all the numerical values we used in the algorithm :

Name of the constant	Abreviation	Value
Initial valence electron density (cm^{-3})	u	$2.2 \cdot 10^{22}$
Order of the multiphoton process in IR	n_2	6
Multiphoton cross section ($cm^8.s^{-3}$) in IR	σ_2	$1 \cdot 10^{-174}$
Oscillator strength for the CB	f_{CB}	1
Electron effective mass in the CB (kg)	m*	$0.5 \times 9.1 \cdot 10^{-31}$
Electron-phonon scattering rate (s^{-1})	$1/\tau_{e-p}$	$1.5 \cdot 10^{15}$
Electron trapping time (fs)	τ	150
Effective third order susceptibility for IR	$\chi_2^{(3)}$	$5 \cdot 10^{-13}$

The results of the simulation can be seen in Fig.4.6 It can be compared to Fig.3.3 in Fig.4.7.

4.2.2 Energy absorption

In Fig.4.8 are presented the results of the calculation of absorbed energy in Al_2O_3. As can be seen, the amount of absorbed energy (black squares) is mostly

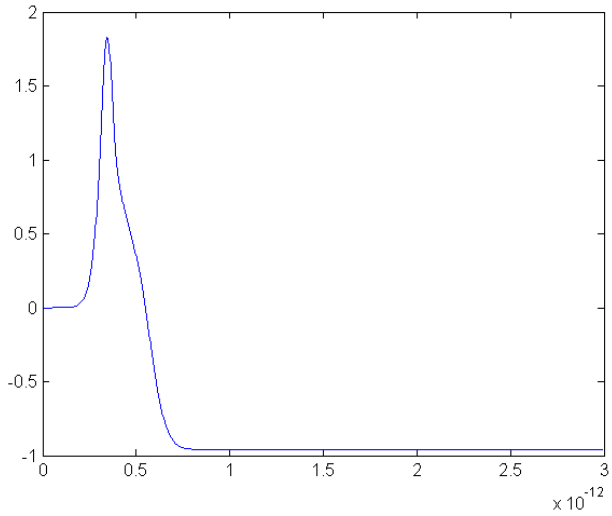

Figure 4.6: Phase in Al_2O_3 for $\lambda = 800$nm

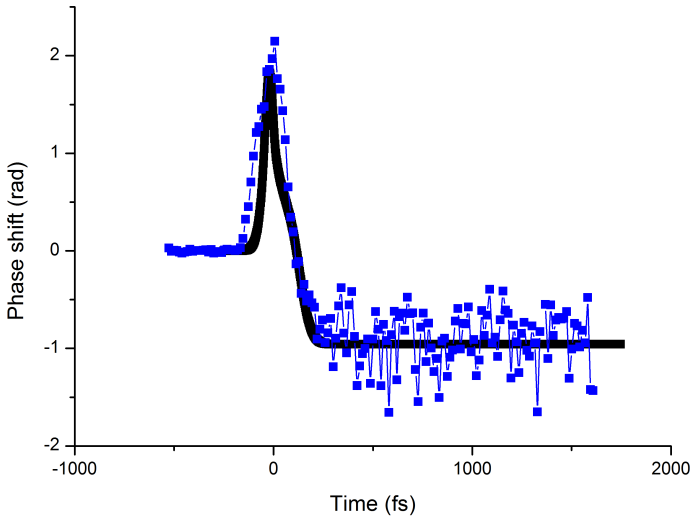

Figure 4.7: Comparison between experimental data and simulation in AlO_2

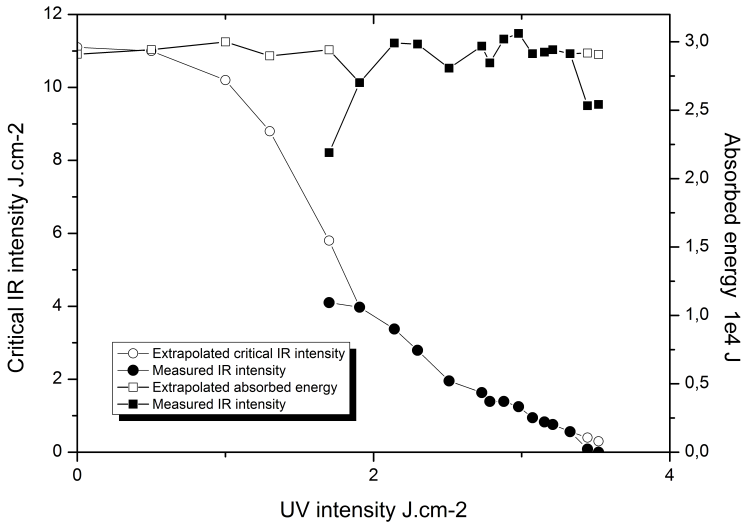

Figure 4.8: Damage threshold in Al2O3 for IR intensity (left scale), and calculated absorbed energy density (right scale)as a function of UV intensity

constant, except for the extreme values of IR intensities (black circle). We also did the inverse calculus, that is to say calculate the IR intensity (empty circle) required to have a constant absorbed energy (empty square). This gives small corrections from the measured intensity, which lies into a reasonable error bar of a few %. This makes absorbed energy the first candidate for an ablation criteria. This is further confirmed by others experiments done in CNRS lab CELIA in Bordeaux. Those results will give birth to an article publication.

4.3 Results for SiO_2

4.3.1 Phase simulation

In table 1 is written all the numerical values we used in the algorithm :

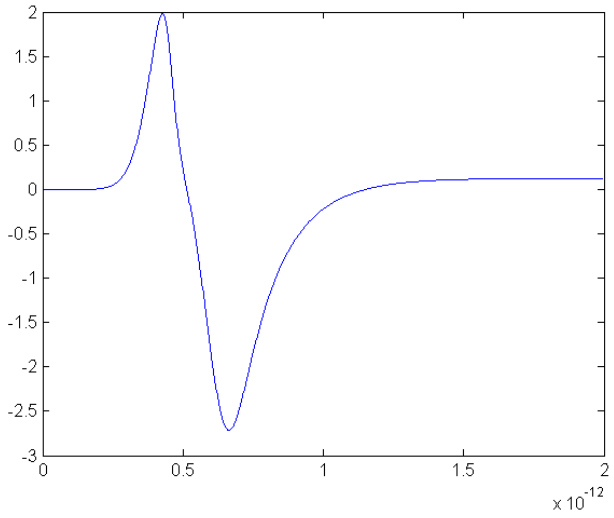

Figure 4.9: Phase in SiO_2 for $\lambda = 800$nm

Name of the constant	Abreviation	Value
Initial valence electron density (cm^{-3})	u	$2.2 \cdot 10^{22}$
Order of the multiphoton process in IR	n_2	6
Multiphoton cross section ($cm^8.s^{-3}$) in IR	σ_2	$10 \cdot 10^{-174}$
Oscillator strength for the CB	f_{CB}	0.005
Electron effective mass in the CB (kg)	m*	$0.5 \times 9.1 \cdot 10^{-31}$
Electron-phonon scattering rate (s^{-1})	$1/\tau_{e-p}$	$1.5 \cdot 10^{15}$
Electron trapping time (fs)	τ	150
Oscillator strength for the first trap level	$f_{tr}^{(1)}$	0.4
Oscillator strength for the second trap level	$f_{tr}^{(2)}$	0.15
First trap level energy (eV)	$\omega_{tr}^{(1)}$	5.2
Second trap level energy (eV)	$\omega_{tr}^{(2)}$	4.2
Width of the first trap level (eV)	$1/\tau_{tr}^{(1)}$	1.5
Width of the second trap leve (eV)	$1/\tau_{tr}^{(2)}$	1
Impact ionization factor	Γ	0.065
One photon cross section (cm^2)	β_2	$1 \cdot 10^{-16}$
One photon cross section (cm^2)	β_3	$1 \cdot 10^{-20}$
Effective third order susceptibility for IR	$\chi_2^{(3)}$	$4 \cdot 10^{-13}$

The simultaion gives Fig.4.9 for SiO_2. It can be compared to the experimental data in Fig.3.1 in fig4.7. As can be seen, the simulation gives very good results.

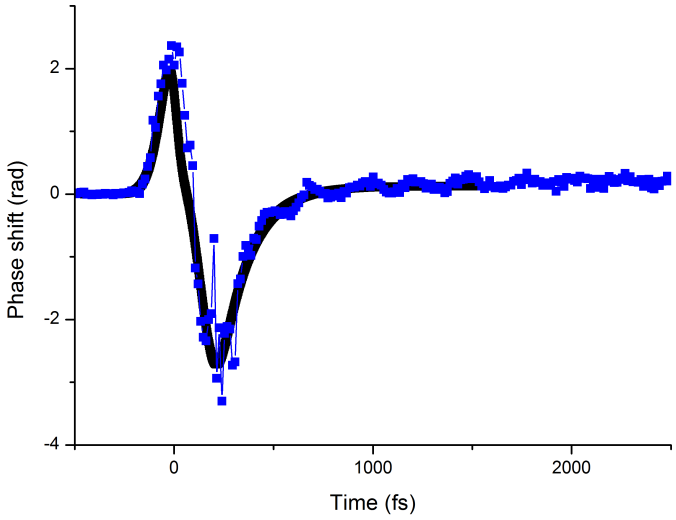

Figure 4.10: Comparison between experimental data and simulation in SiO_2

4.3.2 Energy absorption

In Fig.4.11. is represented the amount of absorbed energy as a function of UV and IR pulse intensity. Again, we see that the absorbed energy is mostly constant, still giving more evidence that it is a good criteria for ablation.

4.4 Transmission measures

Having the same frequency of oscillations in the two experiments would be a good way to confirm that what we see on our data is excited phonons. In Fig.4.12 is a comparison of the oscillations one can find in the phase shift experiment and in the phonons excitation experiment. One can be seen, the two plots can mostly be superposed, and the periods of oscillations are mostly thse same. This is a strong hint that the oscillations are indeed due to phonons. Further experiments are planned to have a definitive answer.

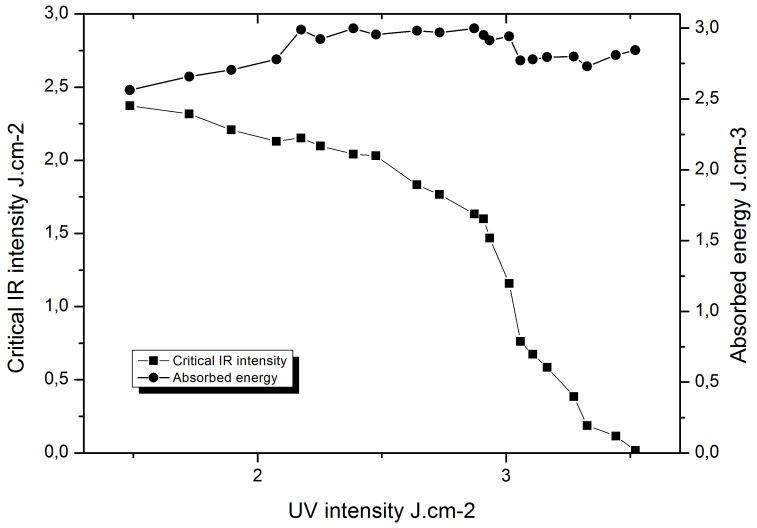

Figure 4.11: Damage threshold in SiO_2 for IR intensity (left scale), and calculated absorbed energy density (right scale)as a function of UV intensity

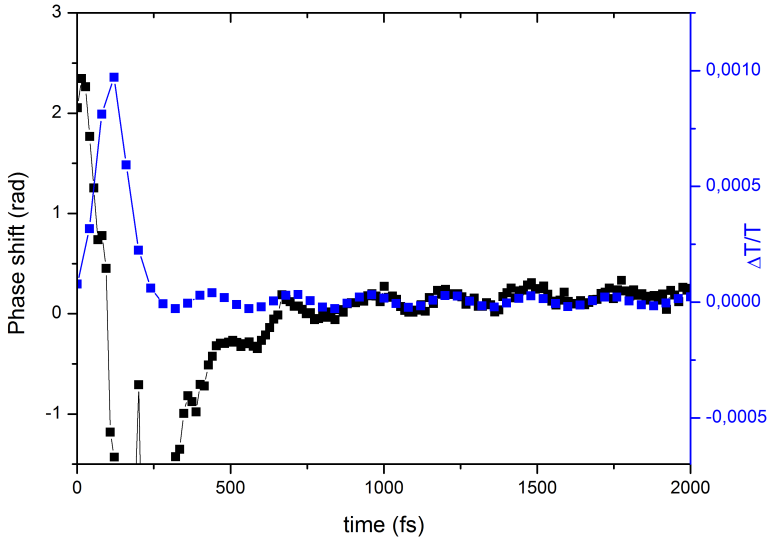

Figure 4.12: Phase shift (left) and transmission (right) vs time

Conclusion

With the frequential interferometry technique using femtosecond laser pulses in a pump-pulse experiment, we were able to follow the dynamics of excited electrons in SiO_2 and Al_2O_3, from the excitations processes to the relaxation processes. We measured the lifetime of the auto-induced excitons created in SiO_2, and we simulated the dynamics of electrons. This gave us the opportunity to calculate the amount of energy absorbed during the propagation of the pulse inside the material, which made us question the ablation criteria. Indead, it does seem like absorbed energy is a better ablation criteria than the excited density. We also made an experiment where we excited phonons, and showed that the period of oscillations is the same as the one in frequential interferometry, which seems to show that we are also extiting phonons.

Further experiments will come in order to gather more proofs that absorbed energy is indeed a better ablation criteria than the excitation density and that multiphoton absorption is the most efficient excitation process. Moreover, it would also be interesting to see if the same effects occur in the bulk of the material when instead of focusing the beams on the surface of the sample, we focus into the bulk.

Annex

A. The final code

First we need to create the adaptative mesh. Here is the code for that :

```
%-------------------------------------------------------------------------
                        %Mesh Creation

i0=1;
j0=1;
theta=pi/2-35*2*pi/360;
CC=cell(1,51);

if theta<pi/4
    x=0;
    y=L;
    p=0;

    while y>=0 && p<2
        y0=y;
        while y0>=0 && x<=L && y0<=LWe
            M(1,j0)=x;
            M(2,j0)=y0;
            j0=j0+1;
            x=x+hx*cos(theta);
            y0=y0+hy*sin(theta);
        end
        CC{1,i0}=M(:,:);
        M=[];
        y=y-sqrt(2*(hx^2+hy^2));
        if y<0
            y=0;
            p=p+1;
        end
        j0=1;
        i0=i0+1;
        x=0;
    end

        nbrPy=i0;
    x=sqrt(2*(hx^2+hy^2))/tan(theta);
    y=0;

    while x<=L
        x0=x;
        while x0<=L && y<=L
            M(1,j0)=x0;
            M(2,j0)=y;
```

```
            j0=j0+1;
            x0=x0+hx*cos(theta);
            y=y+hy*sin(theta);
        end
        CC{1,i0}=M(:,:);
        M=[];
        x=x+sqrt(2*(hx^2+hy^2))/tan(theta);
        j0=1;
        i0=i0+1;
        y=0;
    end

    nbrPx=i0-nbrPy;

else

    x=L;e-174
    y=0;
    p=0;

    while x>=0 && p<2
        x0=x;
        while x0>=0 && y<=L && x0<=L
            M(1,j0)=x0;
            M(2,j0)=y;
            j0=j0+1;
            x0=x0+hx*cos(theta);
            y=y+hy*sin(theta);
        end
        CC{1,i0}=M(:,:);
        M=[];
        x=x-sqrt(2*(hx^2+hy^2))
        if x<0
            x=0;
            p=p+1;
        end
        j0=1;
        i0=i0+1
        y=0;
    end

        nbrPx=i0;
    y=sqrt(2*(hx^2+hy^2))*tan(theta);
    x=0;

    while y<=L
        y0=y;
        while y0<=L && x<=L
            M(1,j0)=x;
            M(2,j0)=y0;
            j0=j0+1;
            x=x+hx*cos(theta);
            y0=y0+hy*sin(theta);
        end
        CC{1,i0}=M(:,:);
        M=[];
        y=y+sqrt(2*(hx^2+hy^2))*tan(theta);
        j0=1;
        i0=i0+1;
        x=0;
    end
        nbrPy=i0- nbrPx;
end
```

Then we shall create the path of the probe :

```
%
    ------------------------------------------------------------------------------

                                Probe initiation

the=pi/2-45*2*pi/360;              % Incoming Angle of the probe
nn=0;
frac=tan(the)*cos(theta)/(sin(theta)+cos(theta)*tan(the));
nnn=frac*(abs(CC{2}(1,1)-CC{1}(1,1)))/(hy*cos(theta));
p=1;
ly=CC{nbrPx-1}(2,2)-CC{nbrPx-1}(2,1);
lx=CC{nbrPx-4}(1,1)-CC{nbrPx-3}(1,1);
nbrPoint=approche((tan(the)*lx)/ly);

for i0=1:length(CC)/2
    if abs(nnn-approche(nnn))<=0.3
        nn=approche(nnn);
        p=i0;

        break;
    else
        nnn=frac*(abs(CC{2+i0}(1,1)-CC{1}(1,1)))/(hy*cos(theta));
    end
end

%
    ------------------------------------------------------------------------------

                              %Probe creation
a=0;
b=0;
a1=0;
b1=0;

absxy=cell(1,20);
coeffxy=cell(1,20);
rr=0;
b=0;
i0=0;
j0=0;
for r0=length(CC):-1:1
    if theta==pi/2 && the~=0
        for m0=0:500
            if 1+m0*p>length(CC)
                f=m0;
                break
            else
                if 1+rr*nn+nn*(m0)>=length(CC{1+m0*p})
                    f=m0;
                    break
                else
                    absxy{rr+1}(1,m0+1)=CC{1+m0*p}(1,1+rr*nn+nn*(m0));
                    absxy{rr+1}(2,m0+1)=CC{1+m0*p}(2,1+rr*nn+nn*(m0));
                    coeffxy{rr+1}(1,m0+1)=1+m0*p;
                    coeffxy{rr+1}(2,m0+1)=1+rr*nn+nn*(m0);
                    b=1;
                end
            end
        end
    elseif the==0 && tetha==pi/2
        rr=0;
    else
        [a,b]=size(CC{r0});
        if abs(CC{r0}(1,b)-L)<0.001
```

```
                for m0=0:500
                    if theta~=pi/2
                        if r0+m0*p>length(CC)
                            f=m0;
                            break
                        else
                            s=approche(CC{r0+m0*p}(2,1)/(1*ly));
                            [a1,b1]=size(CC{r0+p*m0});
                            if b+m0*nn-s>b1 || b+m0*nn-s<=0
                                f=m0;
                                break
                            else
                                absxy{rr}(1,m0+1)=CC{r0+m0*p}(1,b+m0*nn-s);
                                absxy{rr}(2,m0+1)=CC{r0+m0*p}(2,b+nn*m0-s);
                                coeffxy{rr}(1,m0+1)=r0+m0*p;
                                coeffxy{rr}(2,m0+1)=b+nn*m0-s;
                                b=1;
                            end
                        end
                    end
                    pop=m0;
                end
            end
        end
        if b==1
            rr=rr+1;
        end
        b=0;
    end

    if theta==pi/2
        if length(absxy)/2==floor(length(absxy)/2)
            for i0=1:length(absxy)/2

                M=absxy{i0};
                absxy{i0}=absxy{length(absxy)+1-i0};
                absxy{length(absxy)+1-i0}=M;
                M=coeffxy{i0};
                coeffxy{i0}=coeffxy{length(coeffxy)+1-i0};
                coeffxy{length(coeffxy)+1-i0}=M;
                M=[];
            end
        else
            for i0=1:length(absxy)/2-0.5

                M=absxy{i0};
                absxy{i0}=absxy{length(absxy)+1-i0};
                absxy{length(absxy)+1-i0}=M;
                M=coeffxy{i0};
                coeffxy{i0}=coeffxy{length(coeffxy)+1-i0};
                coeffxy{length(coeffxy)+1-i0}=M;
                M=[];
            end
        end
    end

    b=0;
    for r0=1:length(CC)
        if the~=pi/2
            for m0=0:500
                if r0+m0*p>length(CC)
                    f=m0;
                    break
                else
                    s=approche(CC{r0+m0*p}(2,1)/(1*ly));
                    if 1+m0*nn-s<=0 || 1+m0*nn-s>length(CC{r0+m0*p})
                        f=m0;
                        break
```

```
                else

                    absxy{rr}(1,m0+1)=CC{r0+m0*p}(1,1+nn*m0-s);
                    absxy{rr}(2,m0+1)=CC{r0+m0*p}(2,1+nn*m0-s);
                    coeffxy{rr}(1,m0+1)=r0+m0*p;
                    coeffxy{rr}(2,m0+1)=1+m0*nn-s;
                    b=1;
                end
            end
        end
    else
        for m0=0:500
            if m0+1>length(CC{r0})
                break
            else
                absxy{rr}(1,m0+1)=CC{r0}(1,m0+1);
                absxy{rr}(2,m0+1)=CC{r0}(2,m0+1);
                coeffxy{rr}(1,m0+1)=r0;
                coeffxy{rr}(2,m0+1)=m0+1;
                b=1;
            end
        end
    end
    if b==1
        rr=rr+1;
    end
    b=0;
    % [r0,r0+m0*p,length(CC),1+m0*nn-s, length(CC{r0})]
end
```

The two pump pulses are then created :

```
%-------------------------------------------------------------------------
                                Initialization of the pump pulses
for dt=0:ht:ht*nt-ht
FFp1(1,f)=(I01/(h*wl1))*exp(-(dt-tarrivee1)^2/(2*sig1^2))*exp(-(xarrivee1-xarrivee1)^2/(2*sigx1^2));
FFp2(1,f)=(I02/(h*wl2))*exp(-(dt-tarrivee2)^2/(2*sig2^2))*exp(-(xarrivee2-xarrivee2)^2/(2*sigx2^2));
        f=f+1;
end
```

And finally the algorithm occurs :

```
for i0=1:length(CC)
    for dt=1:nt-1
        for dy=1:length(CC{i0})-1
            if Nv(dy,dt)==0;
                PIIP=0;
            end
            NN(dy,dt+1)=2*PIIP*FFp2(dy,dt)*h*wl2*ht*NN3(dy,dt)-beta2*ht*NN(dy,dt)*FFp2(dy,dt)
                        -beta1*ht*NN(dy,dt)*FFp1(dy,dt)+ht*sigma1*Nv(dy,dt)*FFp1(dy,dt)^np1
                        +ht*sigma2*Nv(dy,dt)*FFp2(dy,dt)^np2-ht*NN(dy,dt)/tau+NN(dy,dt)
                        +ht*2*NNtr(dy,dt)*sigma3*FFp2(dy,dt)^np3;
            if NN(dy,dt+1)>u
```

```
    0
    [i0,dy,dt]
    return
end

NNtr(dy,dt+1)=ht*NN(dy,dt)/tau+ht*NN3(dy,dt)/tau+NNtr(dy,dt)
              -ht*2*NNtr(dy,dt)*sigma3*FFp2(dy,dt)^np3+ht*NN2(dy,dt)/tau;
NN2(dy,dt+1)=-beta22*ht*NN2(dy,dt)*FFp2(dy,dt)-beta12*ht*NN2(dy,dt)*FFp1(dy,dt)
              +beta2*ht*NN(dy,dt)*FFp2(dy,dt)+beta1*ht*NN(dy,dt)*FFp1(dy,dt)+NN2(dy,dt)
              -ht*NN2(dy,dt)/tau;
NN3(dy,dt+1)=+beta22*ht*NN2(dy,dt)*FFp2(dy,dt)+beta12*ht*NN2(dy,dt)*FFp1(dy,dt)
              +NN3(dy,dt)-h*wl2*FFp2(dy,dt)*PIIP*ht*NN3(dy,dt)-ht*NN3(dy,dt)/tau;
Nv(dy,dt+1)=u-NN(dy,dt+1)-NNtr(dy,dt+1)-NN2(dy,dt+1)-NN3(dy,dt+1)
              -FFp2(dy,dt)*PIIP*ht*NN3(dy,dt)*h*wl2;

if NNtr(dy,dt+1)<0
    NNtr(dy,dt+1)=0;
    NN(dy,dt+1)=NNtr(dy,dt)+2*h*wl2*FFp2(dy,dt)*PIIP*ht*NN2(dy,dt)
                -beta2*ht*NN(dy,dt)*FFp2(dy,dt)-beta1*ht*NN(dy,dt)*FFp1(dy,dt)
                -ht*NN(dy,dt)/tau+NN(dy,dt)+ht*2*NNtr(dy,dt)*sigma3*FFp2(dy,dt)^np3
                +ht*sigma1*Nv(dy,dt)*FFp1(dy,dt)^np1
                +ht*sigma2*Nv(dy,dt)*FFp2(dy,dt)^np2;
    Nv(dy,dt+1)=u-NN(dy,dt+1)-NNtr(dy,dt+1)-NN2(dy,dt+1)-NN3(dy,dt+1)
                -FFp2(dy,dt)*PIIP*ht*NN3(dy,dt)*h*wl2;
end

if Nv(dy,dt)==0;
    Nv(dy,dt+1)=0;
end

if NN(dy,dt+1)<0
    NN(dy,dt+1)=0;
    NN2(dy,dt+1)=NN(dy,dt)-beta22*ht*NN2(dy,dt)*FFp2(dy,dt)
                -beta12*ht*NN2(dy,dt)*FFp1(dy,dt)+NN2(dy,dt)-ht*NN2(dy,dt)/tau;
    NN3(dy,dt+1)=+beta22*ht*NN2(dy,dt)*FFp2(dy,dt)+beta12*ht*NN2(dy,dt)*FFp1(dy,dt)
                +NN3(dy,dt)-h*wl2*FFp2(dy,dt)*PIIP*ht*NN3(dy,dt)-ht*NN3(dy,dt)/tau;
    NNtr(dy,dt+1)=NNtr(dy,dt)-ht*2*NNtr(dy,dt)*sigma3*FFp2(dy,dt)^np3
                +ht*NN2(dy,dt)/tau+ht*NN3(dy,dt)/tau;
    Nv(dy,dt+1)=u-NN(dy,dt+1)-NNtr(dy,dt+1)-NN2(dy,dt+1)-NN3(dy,dt+1)
                -FFp2(dy,dt)*PIIP*ht*NN3(dy,dt)*h*wl2;
end

if Nv(dy,dt+1)<0
    Nv(dy,dt+1)=0;
    PIIP=0;
    NN(dy,dt+1)=Nv(dy,dt)+2*h*wl2*FFp2(dy,dt)*PIIP*ht*NN2(dy,dt)
                -beta2*ht*NN(dy,dt)*FFp2(dy,dt)-beta1*ht*NN(dy,dt)*FFp1(dy,dt)
                -ht*NN(dy,dt)/tau+NN(dy,dt)+ht*2*NNtr(dy,dt)*sigma3*FFp2(dy,dt)^np3;
    NNtr(dy,dt+1)=ht*NN3(dy,dt)/tau+ht*NN(dy,dt)/tau+NNtr(dy,dt)
                -ht*2*NNtr(dy,dt)*sigma3*FFp2(dy,dt)^np3+ht*NN2(dy,dt)/tau;
    NN2(dy,dt+1)=-beta22*ht*NN2(dy,dt)*FFp2(dy,dt)-beta12*ht*NN2(dy,dt)*FFp1(dy,dt)
                +beta2*ht*NN(dy,dt)*FFp2(dy,dt)+beta1*ht*NN(dy,dt)*FFp1(dy,dt)
                +NN2(dy,dt)-h*wl2*FFp2(dy,dt)*PIIP*ht*NN2(dy,dt)-ht*NN2(dy,dt)/tau;
    NN3(dy,dt+1)=+beta22*ht*NN2(dy,dt)*FFp2(dy,dt)+beta12*ht*NN2(dy,dt)*FFp1(dy,dt)
                +NN3(dy,dt)-h*wl2*FFp2(dy,dt)*PIIP*ht*NN3(dy,dt)-ht*NN3(dy,dt)/tau;

    if NN(dy,dt+1)<0
        NN(dy,dt+1)=0;
        NN2(dy,dt+1)=Nv(dy,dt)+NN(dy,dt)-beta22*ht*NN2(dy,dt)*FFp2(dy,dt)
                -beta12*ht*NN2(dy,dt)*FFp1(dy,dt)+NN2(dy,dt)-ht*NN2(dy,dt)/tau;
        NN3(dy,dt+1)=+beta22*ht*NN2(dy,dt)*FFp2(dy,dt)+beta12*ht*NN2(dy,dt)*FFp1(dy,dt)
                +NN3(dy,dt)-h*wl2*FFp2(dy,dt)*PIIP*ht*NN3(dy,dt)-ht*NN3(dy,dt)/tau;
        NNtr(dy,dt+1)=NNtr(dy,dt)-ht*2*NNtr(dy,dt)*sigma3*FFp2(dy,dt)^np3
                +ht*NN2(dy,dt)/tau+ht*NN3(dy,dt)/tau;
    end
    g=g+1;
end
```

```
            Eepsilon2(dy,dt)=1+Nv(dy,dt)*f12*Depl+FFp1(dy,dt)*h*wl1*chi31+FFp2(dy,dt)*h*wl2*chi32
                    +(ee^2/epsilon0)*(-(NN(dy,dt)+NN2(dy,dt)+NN3(dy,dt))*FreeE2+NNtr(dy,dt)*(Tr21));
                if imag(sqrt(Eepsilon2(dy,dt)))==-inf
                    disp('Erreur, infinité')
                    3
                    [i0,dy,dt]
                    return
                end
                FFp1(dy+1,dt)=-hy*Nv(dy,dt)*np1*h*wl1*sigma1*FFp1(dy,dt)^np1
                              -(2*hy*wl1/c)*imag(sqrt(Eepsilon2(dy,dt)))*FFp1(dy,dt)+FFp1(dy,dt);

                if FFp2(dy+1,dt)==inf
                    disp('Erreur, infinité')
                    2
                    [i0,dy,dt]
                    return
                end

            FFp2(dy+1,dt)=-hy*Nv(dy,dt)*np2*h*wl2*sigma2*FFp2(dy,dt)^np2
                    -(2*hy*wl2/c)*imag(sqrt(Eepsilon2(dy,dt)))*FFp2(dy,dt)+FFp2(dy,dt);
                if FFp1(dy+1,dt)==inf
                    disp('Erreur, infinité')
                    1
                    [i0,dy,dt]
                    return
                end
                ord1(dy,dt)=real(sqrt(Eepsilon2(dy,dt)))-n0;
                ord2(dy,dt)=beta12*NN2(dy,dt)*h*wl1*FFp1(dy,dt)+beta22*NN2(dy,dt)*h*wl2*FFp2(dy,dt)
                            +beta1*NN(dy,dt)*h*wl1*FFp1(dy,dt)+beta2*NN(dy,dt)*h*wl2*FFp2(dy,dt)
                            +(2*wl1/c)*imag(sqrt(Eepsilon2(dy,dt)))*(FFp1(dy,dt)*wl1*h)
                            +(2*wl2/c)*imag(sqrt(Eepsilon2(dy,dt)))*(FFp2(dy,dt)*wl2*h)
                            +2*np3*h*wl2*sigma3*FFp2(dy,dt)^np3;
                PIIP=PII;
            end
            dt
        end

        for dt=1:length(t)-1
            deltaphi(1,dt)=(2*pi/lambda2)*trapz(yy1,ord1(:,dt));
        end


        for dy=1:length(CC{i0})-1
            EE(1,dy)=trapz(t,ord2(dy,:));
        end
      Etot=trapz([0:ly:length(CC{i0})*ly-2*ly],EE(1,:))/Ly;
    end
```

As can be seen, the code is much more complex than for the 1D algorithm, because they are more phenomena to simulate, and because we also added control sequences, so that for example the algorithm can handle the case when there is no more electrons in the valence band.

Bibliography

[1] Hengchang Guo, Hongbing Jiang, Ying Fang, Chao Peng, Hong Yang, Yan Li, and Qihuang Gong. The pulse duration dependence of femtosecond laser induced refractive index modulation in fused silica. *Journal of Optics A: Pure and Applied Optics*, 6(8):787, August 2004.

[2] M. Ams, G. D. Marshall, P. Dekker, M. Dubov, V. K. Mezentsev, I. Bennion, and M. J. Withford. Investigation of ultrafast laser photonic material interactions: challenges for directly written glass photonics. *IEEE Journal of Selected Topics in Quantum Electronics*, 14(5):1370–1381, 2008. arXiv:0802.1966 [physics].

[3] Mykhaylo Dubov, Vladimir Mezentsev, and Ian Bennion. Femtosecond inscription of the first order bragg gratings in pure fused silica. *Nano Science and technology institute*, 2006.

[4] Christian Voigtländer, Daniel Richter, Jens Thomas, Andreas Tünnermann, and Stefan Nolte. Inscription of high contrast volume bragg gratings in fused silica with femtosecond laser pulses. *Applied Physics A*, 102(1):35–38, January 2011.

[5] Martynas Beresna, Mindaugas Gecevi?ius, and Peter G. Kazansky. Polarization sensitive elements fabricated by femtosecond laser nanostructuring of glass [invited]. *Optical Materials Express*, 1(4):783–795, August 2011.

[6] Yasuhiko Shimotsuma, Kazuyuki Hirao, Peter G. Kazansky, and Jiarong Qiu. Three-dimensional micro- and nano-fabrication in transparent materials by femtosecond laser. *Japanese Journal of Applied Physics*, 44(7A):4735–4748, 2005.

[7] B. C. Stuart, M. D. Feit, S. Herman, A. M. Rubenchik, B. W. Shore, and M. D. Perry. Nanosecond-to-femtosecond laser-induced breakdown in dielectrics. *Physical Review B*, 53(4):1749–1761, January 1996.

[8] Mark Fox. *Optical Properties of Solids*. OUP Oxford, March 2010.

[9] Katsumi Tanimura, Takeshi Tanaka, and Noriaki Itoh. Creation of quasistable lattice defects by electronic excitation in SiO2. *Physical Review Letters*, 51(5):423–426, August 1983.

[10] C. Itoh, K. Tanimura, and N. Itoh. Optical studies of self-trapped excitons in SiO2. *Journal of Physics C: Solid State Physics*, 21(26):4693, September 1988.

[11] F. Quéré, S. Guizard, and Ph Martin. Time-resolved study of laser-induced breakdown in dielectrics. *EPL (Europhysics Letters)*, 56(1):138, October 2001.

[12] S. Guizard, A. Semerok, J. Gaudin, M. Hashida, P. Martin, and F. Quéré. Femtosecond laser ablation of transparent dielectrics: measurement and modelisation of crater profiles. *Applied Surface Science*, 186(1-4):364–368, January 2002.

[13] Scott C. Jones, Peter Braunlich, R. Thomas Casper, Xiao-An Shen, and Paul Kelly. Recent progress on laser-induced modifications and intrinsic bulk damage of wide-gap optical materials. *Optical Engineering*, 28(10):281039–281039–, 1989.

[14] Guillaume Petite. Mécanismes fondamentaux de l'ablation laser femtoseconde en flux intermédiaire. 2005.

[15] B. K. Ridley. *Quantum Processes in Semiconductors*. OUP Oxford, November 1999.

[16] D. Arnold, E. Cartier, and D. J. DiMaria. Theory of high-field electron transport and impact ionization in silicon dioxide. *Physical Review B*, 49(15):10278–10297, April 1994.

[17] S. Guizard, P. Martin, G. Petite, P. D'Oliveira, and P. Meynadier. Time-resolved study of laser-induced colour centres in SiO2. *Journal of Physics: Condensed Matter*, 8(9):1281, February 1996.

[18] Yong-Xin Yan, Edward B. Gamble Jr, and Keith A. Nelson. Impulsive stimulated scattering: General importance in femtosecond laser pulse interactions with matter, and spectroscopic applications. *The Journal of Chemical Physics*, 83(11):5391–5399, December 1985.

[19] Robert W. Boyd. *Nonlinear Optics*. Academic Press, January 2003.

[20] Ajit P. Joglekar, Hsiao-hua Liu, Edgar Meyhöfer, Gerard Mourou, and Alan J. Hunt. Optics at critical intensity: Applications to nanomorphing. *Proceedings of the National Academy of Sciences of the United States of America*, 101(16):5856–5861, April 2004.

[21] R. Stoian, D. Ashkenasi, A. Rosenfeld, and E. E. B. Campbell. Coulomb explosion in ultrashort pulsed laser ablation of al2o3. *Physical Review B*, 62(19):13167–13173, November 2000.

[22] B. Chimier, O. Utéza, N. Sanner, M. Sentis, T. Itina, P. Lassonde, F. Légaré, F. Vidal, and J. C. Kieffer. Damage and ablation thresholds of fused-silica in femtosecond regime. *Physical Review B*, 84(9):094104, September 2011.

[23] Philippe Daguzan. *Dynamique ultra-rapide des porteurs photoexcités dans les solides à grande bande interdite*. PhD thesis, Université Paris 6, 1996.

[24] Alexandros Mouskeftaras. *Study of the physical mechanisms involved in the femtosecond laser optical breakdown of dielectric materials*. PhD thesis, Ecole Polytechnique, 2013.

[25] P. Martin, S. Guizard, Ph. Daguzan, G. Petite, P. D'Oliveira, P. Meynadier, and M. Perdrix. Subpicosecond study of carrier trapping dynamics in wide-band-gap crystals. *Physical Review B*, 55(9):5799–5810, March 1997.

[26] X. Yu, Q. Bian, B. Zhao, Z. Chang, P. B. Corkum, and S. Lei. Near-infrared femtosecond laser machining initiated by ultraviolet multiphoton ionization. *Applied Physics Letters*, 102(10):101111, March 2013.

[27] Davide Boschetto. *Etude par spectroscopie visible et diffraction X résolues en temps de phonons optiques cohérents*. PhD thesis, Ecole Polytechnique, 2004.

[28] B. Rethfeld. Free-electron generation in laser-irradiated dielectrics. *Physical Review B*, 73(3):035101, January 2006.